ISSN 0915-633X

NATIONAL INSTITUTE FOR FUSION SCIENCE

Condensation and Swelling Behavior of Randomly Charged Multichain Polymers by Molecular Dynamics Simulations

M. Tanaka, A.Yu Grosberg and T. Tanaka

(Received - Nov. 16, 1999)

NIFS-616 Dec. 1999

This report was prepared as a preprint of work performed as a collaboration reserch of the National Institute for Fusion Science (NIFS) of Japan. This document is intended for infomation only and for future publication in a journal after some rearrangements of its contents.

Inquiries about copyright and reproduction should be addressed to the Research Information Center, National Institute for Fusion Science, Oroshi-cho, Toki-shi, Gifu-ken 509-02 Japan.

RESEARCH REPORT
NIFS Series

NAGOYA, JAPAN

Condensation and Swelling Behavior of Randomly Charged Multichain Polymers by Molecular Dynamics Simulations

Motohiko Tanaka*, A.Yu Grosberg[1], and Toyoichi Tanaka[2]

National Institute for Fusion Science, Toki 509-5292, Japan
[1]Dept. of Physics, University of Minnesota, Minneapolis, MN 55455
[2]Dept. of Physics, Massachusetts Institute of Technology, Cambridge, MA 02139

Abstract

The behavior of polyampholytes over a wide range of temperatures is studied with the use of molecular dynamics simulations. It has been found that biased fluctuations of charge density due to aggregation of oppositely charged monomers causes the Coulombic interactions more attractive than repulsive for a globally near-neutral polyampholyte. Such a polyampholyte collapses to a globule, in which the polymer chains inter-penetrate with each other and reptate through the whole globule. It further condenses to an NaCl-like cubic crystal for widely extensible chains, but crystallization is suppressed for finite extensible chains. Hysteresis in the volume-temperature diagram is prominent for multichain polyampholytes, which is absent for individual chains. Multichain effects always dominate over the single-chain effects in swelling processes of polyampholytes. A non-neutral polyampholyte still forms a globule if the amount of charge offset is less than $\frac{1}{2}N^{1/2}$ (N: the number of charged monomers) at low temperatures. Otherwise, it consists of scattered chains and is swollen. At high temperatures, it shrinks to the thermal state where the Coulomb force plays little role. A polyampholyte with slight charge offset has a non-monotonic (re-entrant) phase boundary with temperature. These results in the temperature domain are in good agreement with polyampholyte experiments with variable salt concentrations.

Keywords: condensation, reptation, Coulombic crystal, hysteresis, multichain, reentrant volumetric change, salt and temperature effects, molecular dynamics.

*Present address: Max-Planck Institut für Polymerforschung, Ackermannweg 10, D-55128 Mainz, Germany

1. Introduction

Condensation and swelling behavior against temperature and salt ionic strength are important subjects of polyampholytes, which are heterogeneous polymers consisting of linked monomers of both positive and negative charges[1]. A study on these subjects offers us informations of thermodynamical and dynamical properties of polyampholytes, including their internal structures of formed charge complexes (aggregates), the way of chain reptation in a globule, and stability of such structures. This clarifies the roles of long-range Coulomb forces in a constrained heterogeneous charged system of three dimensions.

The Coulomb forces have both repulsive and attractive parts for polyampholytes. The former arises from unbalanced excess charges, and is predominant for non-neutral polyampholytes. The latter arises from biased charge density fluctuations due to the formation of charge complexes of positive and negative monomers. Resultant interactions between the electric dipoles of the complexes are attractive. The formation of such complexes was directly measured[7], and is better seen in the pair correlation functions in this paper. Moreover, we should note that the attractive force overcomes the repulsive force for block copolymers with alternating charged blocks whose chains are all neutral (cf. Fig.7 of Ref.7).

The statistical properties of the *single-chain* polyampholytes were well studied in the framework of Debye-Hückel theory[2], and the Flory-type free energy theory[3]. An early numerical study of single-chain polyampholytes was performed by the Monte Carlo simulations under a lattice model[4]. It found a collapsed globule for neutral polyampholytes and a self-avoiding stretched coil for non-neutral polyampholytes. Later, the importance of multichain effects in the semi-dilute and dense regimes of polyampholyte solution was pointed out analytically, which showed the limitation of the single-chain theories in realistic applications[5].

Statistical and dynamical properties of polyampholytes for both the single-chain[6] and multichain[7] cases were investigated with the molecular dynamics simulations in the full three-dimensional space (non-lattice model). Another molecular dynamics simulation was done to examine the effect of applied electric field on the stretching behavior of polyampholyte[8].

In the former studies by molecular dynamics simulations[6,7], a very compact and dense globular state was discovered by means of the non-lattice model. It was shown that the attractive nature of the Coulomb forces for the globally neutral polyampholyte arises from the formation of complexes of positive and negative monomer pairs. A multichain polyampholyte showed larger swelling than its single-chain counterpart because of creation of large void space among the chains[7]. Thermodynamical stability of the globule at low temperatures against thermal agitations was proved numerically and theoretically. Also, salt ions were demonstrated to disintegrate a collapsed globule by migrating inside and screening the electric field; dynamical processes including the relaxation time were shown to be adequately studied only by kinetic tools such as molecular dynamics simulations[7].

Experimentally, the swelling behavior of polyampholyte polymers and gels has been studied by changing salt concentration over several orders of magnitude at fixed temperature[9–11]. There, it was shown that globally neutral polyampholytes occupy small volumes at low salt concentration, and swell monotonically with addition of salt. By contrast, non-neutral polyampholytes are swollen at low salt concentration, and they shrink to the same volume as that of the neutral ones at high salt concentration.

The low temperature behavior of non-neutral polyampholytes was previously studied by the Monte Carlo simulations[4]. However, these simulations considered only single-chain cases and adopted the lattice model, which becomes very inaccurate as monomers are condensed at low temperatures. For this reason, numerical studies in the full three-dimensional space are more appropriate.

In passing, we remark similar controlling roles of temperature and salt ionic strength. The major role of the salt ions is screening of the electric field, which modifies the electrostatic potential as $\varphi \sim (1/r)\exp(-r/\lambda_s)$, where $\lambda_s = (\epsilon k_B T/4\pi e^2(Z_s^2 n_s + n_0))^{1/2}$ is the Debye screening length in the presence of salt ions, with ϵ electrical permitivity of surrounding medium, k_B the Boltzmann constant, T temperature, e the unit charge, n_s and Z_s the density and valence of salt ions, n_0 the density of polyampholyte. This reduces the electrostatic energy by a factor $(\lambda_s/\lambda_D)^2 \sim 1/(1+Z_s^2 n_s/n_0)$. Thus, the electrostatic coupling constant, which is the ratio of the electrostatic energy to that of thermal energy, is modified as

$$\begin{aligned}\Gamma &= (e^2/\epsilon a k_B T)(\lambda_s/\lambda_D)^2 \\ &= (\lambda_B/a)(\lambda_s/\lambda_D)^2 \propto 1/Z_s^2 n_s T,\end{aligned} \quad (1)$$

where a is the unit length, and λ_B the Bjerrum length. The electrostatic coupling constant is the most important parameter to describe the role of the Coulombic interactions in charged systems[6].

In this paper, we will study the behavior of *multichain* polyampholytes, focusing on the effects of temperature (or the Bjerrum length $\lambda_B \sim T^{-1}$) over a wide range, with the use of molecular dynamics simulations. In order to quantify the swellings of polyampholytes, we measure the gyration radius of the system (all chains) $R_{g,sys}$, and that of each chain $R_{g,1}$ averaged over the chains.

$$R_{g,sys} = \left(\frac{1}{N}\sum_{j=1}^{N}(\mathbf{r}_j - <\mathbf{r}>)^2\right)^{1/2}. \quad (2)$$

$$R_{g1} = \frac{1}{N_c}\sum_{s=1}^{N_c}\left(\frac{1}{N_1}\sum_{j=1}^{N_1}(\mathbf{r}_j - <\mathbf{r}_s>)^2\right)^{1/2} \quad (3)$$

where $\mathbf{r}_j$ is the coordinate of the j-th particle, $<\mathbf{r}>$ and $<\mathbf{r}_s>$ are the mass centers of all the monomers and the s-th chain, respectively, and N, N_c and N_1 are the numbers of all the monomers, chains, and monomers per chain, respectively. We define the filling index

$$\zeta = N_c^{1/3} R_{g,1}/R_{g,sys}. \quad (4)$$

The condition $\zeta \geq 1$ means that the chains are overlapped and form a globule, whereas for $\zeta < 1$ the chains are scattered across the whole allowable domain. We also measure the average distance of connected monomers d_{p-p}, the electrostatic energy

$$W_p = \frac{1}{N}\sum_i\sum_{j>i} Z_i Z_j e^2/\epsilon|\mathbf{r}_i - \mathbf{r}_j|, \quad (5)$$

and the time fluctuations of the monomer distance,

$$\delta R = \frac{2}{N(N-1)}\sum_i\sum_{j>i}\delta r_{ij}/<r_{ij}>, \quad (6)$$

where $r_{ij} = |\mathbf{r}_i - \mathbf{r}_j|$, and δr_{ij} is its time (root-mean square) fluctuations.

We will show that, by decreasing temperature, a globally charge-neutral polyampholyte collapses monotonically to a compact globule, in which chains are inter-penetrating with each other and reptating around the whole volume of the globule. By further cooling, it turns into an ordered structure close to the NaCl crystal. The multichain effect is shown to cause polyampholytes much larger volume changes than the single-chain effect does. Irreversibility of the volume change is

a pronounced feature of multichain polyampholyte, which is manifested in hysteresis in the system gyration radius.

Also, the bare behavior of non-neutral polyampholyte in the absence of counterions is studied. Even a non-neutral polyampholyte forms a globule if the global charge offset is less than $N^{1/2}$. Otherwise, it is swollen at low temperatures, and shrinks monotonically to a volume similar to that of the neutral ones at high temperatures. The volumetric changes of slightly non-neutral polyampholyte are reentrant; first shrinking and then swelling with the increase in temperature.

In Sec.2 of this paper, the equations of motion adopted in the present study are given. Condensation behavior of globally charge-neutral polyampholytes at very low temperatures is shown in Sec.3. Swelling behavior of non-neutral polyampholytes is described in Sec.4. Sec.5 will be a summary of this paper. The effects of counterions that neutralize and modify the polyampholyte structure will be studied in the sequel paper.

2. The Equations of Motion

The multichain polyampholytes adopted in this study consist of six 32-mer chains. The initial configurations of the chains are generated by random walks, and the charge sequence on each chain is also picked at random. When the global (overall) charge neutrality constraint is imposed, half the monomers of the whole polyampholyte are assigned positive charges and the other half negative charges. These given charges are then well shuffled in terms of the monomer indices to realize random sequences on any part of the chains. The polyampholytes thus prepared are submerged in a Langevin fluid. The dynamical motions of monomers are governed by the Newton-Langevin equations of motion[6,7],

$$m\frac{d\mathbf{v}_i}{dt} = \mathbf{F}_{LR}(\mathbf{r}_i) - \frac{3k_BT}{a^2}(2\mathbf{r}_i - \mathbf{r}_{i+1} - \mathbf{r}_{i-1}) + \mathbf{F}_{th} - \nu m\mathbf{v}_i - \frac{\partial U_{LJ}}{\partial \mathbf{r}}, \quad (7)$$

$$\frac{d\mathbf{r}_i}{dt} = \mathbf{v}_i. \quad (8)$$

Here, $\mathbf{r}_i$ and $\mathbf{v}_i$ are the position and velocity of the i-th monomer ($i = 1 \sim N$), respectively, m is the monomer mass, T the temperature, a the normalization length (which is close in value to the bond length of the monomer pairs), and ν the friction constant. The Coulomb force $\mathbf{F}_{LR}$, which is an electrostatic long-range force, is obtained by summing over all the possible monomer pairs,

$$\mathbf{F}_{LR}(\mathbf{r}_i) = \sum_j \frac{Z_iZ_je^2}{\epsilon\,|\mathbf{r}_i - \mathbf{r}_j|^2}\hat{\mathbf{r}}_{ij}, \quad (9)$$

where Z_i is a charge state ($Z_i = \pm 1$), ϵ the electrical permitivity, and $\hat{\mathbf{r}}_{ij}$ a unit vector along the line $(\mathbf{r}_i - \mathbf{r}_j)$. The last term of Eq.(7) represents the short-range force (mostly repulsive) due to the Lennard-Jones potential,

$$U_{LJ}(r) = U_0\left\{\left(\frac{a_{LJ}}{r}\right)^{12} - \left(\frac{a_{LJ}}{r}\right)^{6}\right\}, \quad (10)$$

where a_{LJ} is the exclusion radius. Here, we set $a_{LJ} = a$ and $U_0 = e^2/12\epsilon a_{LJ}$; when two monomers make a close encounter of distance $r \sim a_{LJ}$, they repel each other in an elastic fashion. The potential Eq.(10) represents *a good solvent* (the second Virial coefficient is positive) for the temperatures $T/T_0 < 1$.

In Eq.(7), a harmonic spring that is widely extensible is adopted to account for the connection of two adjacent monomers. Combination of *finite extensible bonds and impenetrable monomers (Eq.(4))* are also used in Sec.3 to delineate the effect of monomer bonds in the condensation process. The thermal force $\mathbf{F}_{th}$ that exerts random kicks on the monomers is generated with the use of random numbers with a Gaussian distribution in

each time step. The strength of the thermal kicks is controlled in such a way that the average kinetic energy of the monomer equals $\frac{3}{2}k_BT$ in balance with the momentum absorption by the immobile solvent[6]. (Energy units are hereafter used in which the temperature T stands for k_BT, with k_B the Boltzmann constant.)

Several series of runs are performed for globally neutral and non-neutral polyampholytes that have different initial configurations and charge sequences. Typical charge sequences of the chains of such polyampholytes are tabulated in Table I, which are used in the runs of Figs.1, 3 and 10. To examine the temperature effect, the whole system is cooled gradually as $T(t) = 2^{-t/\tau_0}T_1$. Here, the initial temperature of $T_1 = \frac{1}{2}T_0$ (or the Bjerrum length $\lambda_B = 5a$) is chosen, where T_0 is the base temperature at which the electrostatic and thermal energies are of equal amount at the distance a, i.e. $e^2/\epsilon a T_0 = 1$. Temperature is then gradually raised with the same time constant, by immediately following the first cooling stage to see reciprocality of polyampholyte behaviors for cooling and heating.

The boundary conditions of an isolated charge system are used in this study. The velocity of the monomers hitting a boundary sphere, which is located at the radius $r = 21a$, is inverted in an elastic fashion. The choice of such boundary conditions is justified for studies of physics processes, since it was confirmed in our previous study[12] with the periodic boundary conditions (the Ewald sum method[13]) that the swelling behavior of polyampholytes is only slightly modified compared to those for the isolated system.

3. Swelling Behavior of Neutral Polyampholytes

(a) Reptation and hysteresis

A typical behavior of globally charge-neutral polyampholyte in the cooling stage is shown by filled circles in Fig.1. The behavior of the same polyampholyte in subsequent heating stage is shown by open circles. The time constant of cooling is $\tau_0 = 2000\omega_p^{-1}$, where $\omega_p = (2\pi e^2/\epsilon m a^3)^{1/2}$ is plasma frequency, which becomes $\omega_p \sim 5 \times 10^{-12}\text{sec}^{-1}$ (about 1 psec) for the CH_2 monomer with $a = 3$ Å in water ($\epsilon = 80$). We note that the relaxation time of the given polyampholyte chains is $\tau \sim 300\omega_p^{-1}$.

Six quantities shown in Fig.1 are the system gyration radius of all the chains which represents the multichain effects, $R_{g,sys}$, the average gyration radius of the chains representing the single-chain effects, $R_{g,1}$, the filling index that indicates overlap of the chains $\zeta = N_c^{1/3}R_{g,1}/R_{g,sys}$, the electrostatic energy, $-W_p$ (the sign reversed, $W_p = (1/N)\sum_{i>j} Z_iZ_je^2/\epsilon|\mathbf{r}_i - \mathbf{r}_j|$), the average distance of connected monomers d_{p-p}, and the mean-square distance fluctuations of (all) monomers δR normalized by i the average monomer distance.

For the neutral polyampholyte, two kind of the gyration radii decrease nearly monotonically when temperature is lowered. For $T/T_0 \leq 0.1$ (the Bjerrum length $\lambda_B \geq 10a$), a globule is formed $\zeta \geq 1$. Below this temperature, the change in the gyration radii becomes rather small, which implies that the globule is approaching the highest density state that is allowed to the system. It is quite remarkable that the gyration radius of each chain is close to the system gyration radius, $R_{g,1} \sim R_{g.sys}$. This indicates that the chains are inter-penetrating with each other and reptating through the whole volume of the globule at low temperatures.

The change in the system gyration radius is about a factor of 3.5 in Fig.1, which is twice larger in magnitude than that in the gyration radius of each chain. In terms of the volumetric changes, the multichain effect prevails about ten times over the single-chain effect, which agrees with our previous study[7].

The distance between connected monomers, $d_{p-p} \cong 1.4a$, does not change significantly. A globule that is formed for $T/T_0 < 0.1$ in the cooling stage is kept until higher temperature $T/T_0 \sim 0.3$ (the Bjerrum length $\lambda_B \sim 3a$) in the heating stage. The fluctuations of relative monomer distances δR decrease linearly for $T/T_0 > 0.05$ as temperature is lowered, although the macroscopic quantities such as the gyration radii are rather insensitive to temperature changes for $T/T_0 \leq 0.03$. At very low temperatures $T/T_0 \leq 0.05$, fluctuations decrease as $\delta R \sim T^{1/2}$, and are small but finite, $\delta R/R \sim 10^{-2}$.

Hysteresis in the system gyration radius is seen in Fig.1. The neutral polyampholyte goes along different paths for the cooling and heating stages: the change in the heating stage begins at higher temperature than in the cooling stage. But, hysteresis is absent in the average gyration radius of the chains, which is therefore reversible with temperature. This irreversibility reveals that the globule at low temperatures chooses one of the state out of many possible ones that have almost the same energy. That is, such globule is not thermally equilibrated, and its relaxation should be very slow.

The sign of the electrostatic energy is always negative for neutral polyampholytes, thus indicating the prevalence of attractive Coulomb forces over repulsive ones. As in regular neutral plasma, this so-called *polyampholyte effect* is due to biased fluctuations of charge density. Accordingly, the magnitude of the averaged electrostatic energy, to which the closest pairs of unlike-sign charges most contribute, decreases with temperature, as almost inversely proportional to $\frac{3}{2}$ power of the gyration radius of each chain[3,14], $|W_p| \sim R_{g,1}^{-3/2}$.

It is interesting that, even if the chain bonds between monomers are removed (cut) at very low temperature $T/T_0 \leq 0.001$, the collapsed globule is not destroyed. The globule that has once condensed stays in a stable state under the influence of the Coulomb forces. On the other hand, as one expects, the chain connection makes condensation of polyampholyte smooth and faster under the pressure at which neutral plasma (the system of free charged particles without net charge) of the same density condenses irregularly and slowly (see below).

The behavior of neutral plasma (96 positive and 96 negative particles), that also represents the case of Na^+ and Cl^- gas /liquid, is shown in Fig.2. The charged particles condense in a similar time scale as the polyampholyte only when the size of the simulation domain is cut half, i.e. eight times in density. Clear and smooth hysteresis curves are seen in the volumetric changes for the plasma, since they are not constrained by chain bonds. Condensation takes place at lower temperature than melting occurs at $T/T_0 \sim 10^{-2}$ (or $\Gamma \sim 100$) in the heating stage. We note that multichain environment is required to have hysteresis under the Coulomb forces (cf. Fig.13 of Ref.6).

Figure 3 shows another run for globally neutral polyampholyte of different random sequences. The time constant of the temperature changes is again $\tau_0 = 2000\omega_p^{-1}$. For reference, the heating stage for a plasma - an assembly of free charged particles, is also shown. In the cooling stage, the formation of a globule takes place at the temperature $T/T_0 \sim 0.1$, at which the Bjerrum length is $\lambda_B \sim 10a$. The diameter of the polyampholyte there is close to this length. In the heating stage, the disintegration of the globule occurs slowly and is postponed until higher temperature. These temperatures of the globule formation and disintegration are the same as those in Fig.1, showing the sequence insensitivity.

On the other hand, the plasma begins to deviate from the condensed state even below the temperature $T/T_0 \sim 0.01$; the globule is

rapidly disintegrated above this temperature. The electrostatic energy for the plasma is much reduced when the condensed structure is lost. The stabilizing roles of the chains for polyampholytes are readily seen, as expected, by comparing the curves shown by triangles (plasma) and circles (polyampholyte).

(b) Formation of Coulomb crystal

The bird's-eye view plot of Fig.4 shows the condensed structure, which is seen for the neutral polyampholyte of Fig.3 at the temperature $T/T_0 = 1/512$ in the cooling stage. The red and green spheres represent the positively and negatively charged monomers, respectively, and the upper and lower panels are only different in view angles. There, we see a well ordered structure: the positive and negative monomers are placed in an alternate fashion on vertices of the cubic lattice. Also, the chains are seen to reptate within the structure, connecting one monomer typically with its second-closest or further monomers. This condensed structure is quite similar to the crystal formed in the Na^+ and Cl^- solution, where one Na^+ ion is surrounded by equally spaced six Cl^- ions which are located on vertices of the cubic lattice. In fact, the red and green spheres that are arranged alternately on the cubic lattice look the same as the lower panel of Fig.4 when viewed obliquely from the top side.

Figure 5 depicts the time evolution of the above neutral polyampholyte in the cooling stage. The left panels are bird's-eye view plots of the polyampholyte, and the right panels are the pair correlation functions for the equal-sign pairs G_{++}, and the opposite-sign pairs G_{+-}. At all temperatures, the first peak in $G_{+-}(r)$ is located always inside of the first peak in $G_{++}(r)$. Moreover, the first peak of $G_{+-}(r)$ occurs at the distance r_1 that is significantly shorter than the average bond length of the monomers, $r_1 \cong a_{LJ} < d_{p-p}(\cong 1.4a)$. This confirms reptation of the polymer chains in the condensed structure. These observations also indicate the formation of the positive and negative charge complexes, from which the attractive nature of the Coulomb forces for polyampholytes arises.

The pair correlation function further tells us that the discrete structure becomes evident for the low temperatures $T/T_0 \leq 0.01$ (the Bjerrum length $\lambda_B \geq 100a$). At the temperature $T/T_0 = 1/128$, the polyampholyte is still frustrated, while it becomes highly structured at $T/T_0 = 1/512$. We infer that phase transition from liquid to crystal occurs between these temperatures, namely at $T/T_0 = 0.05$ where the slope of the fluctuations $\delta R/R$ changes. The first peak in $G_{+-}(r)$ occurs at the distance equal to the exclusion radius, $r_1 = a_{LJ}$; the number of monomers at such position is approximately six, which agrees with the case of the cubic lattice. The second neighbors which are the pairs of equal-sign charges sit at $r \sim 1.2a_{LJ}$. Its deviation from the cubic lattice may be due to a small number of monomers in the present globule.

(c) Effect of finite extensible bonds and impenetrable monomers

The NaCl-like cubic lattice was obtained at very low temperature in Fig.1 to Fig.5, as the result of condensation of globally neutral polyampholyte. There, the elastic force was provided by harmonic springs whose force constant was proportional to temperature, $3k_BT/a^2$. Thus, the elastic energy became negligiblly small in comparison with the Coulomb energy at very low temperatures, resulting in the third monomer to penetrate through the connected monomers by pushing them apart.

To see the case of rather rigid chains, another run with the combination of *finite extensible bonds and impenetrable monomers* is performed, in which the largest distance of connected monomers is limited by the length

a_{max}, such that $|\mathbf{r}_i - \mathbf{r}_{i+1}| < a_{max}$. This is realized by providing a high potential $U_{LJ} \gg 0$ beyond a certain length $r < a_{max}$. The result for globally neutral polyampholyte (six 32-mers) with $a_{max} = 1.4a$ is shown in Fig.6. The chains are somewhat more stretched at high and medium temperatures than those of Fig.1, since the chains are more sticky. The average bond length d_{p-p} becomes now shorter at low temperatures. On the other hand, despite such finite extensible chains, the system gyration radius and the average gyration radius decrease rather monotonically when temperature is lowered. The final values of gyration radii are quite comparable to their counterparts in Fig.1.

However, in the bird's-eye view plot of Fig.7, the monomers are seen to overlap rather irregularly. The monomers deviate in space from the positions expected for the cubic lattice, unlike the picture shown in Fig.4. We conclude that significant frustrations are retained in the condensed state of the polyampholyte whose monomers are connected by finite extensible bonds and impenetrable monomers.

If we inspect the pair correlation functions of such polyampholyte shown in Fig.8, the peaks at small distances ($r \leq 2a$) are still located at the same positions as they were in Fig.5. However, a large difference is that these peaks are markedly broad in comparison with those of Fig.5. The number of paired monomers at the peak positions deviates from that of the cubic lattice, except for the nearest-neighbor peak in $G_{+-}(r)$ occurring at $r = a_{LJ}$. The pair correlation functions here resemble those of the neutral polyampholyte just before crystallization (phase transition) at temperature $T/T_0 = 1/128$ of Fig.5. The condensed state for the realistic polyampholyte is only half-ordered, including a lot of frustrations.

4. Swelling Behavior of Non-Neutral Polyampholytes

(a) Monotonic and reentrant swellings

In this section, the effects of unbalanced charges on the volumetric changes of polyampholytes are described. A large number of different sequences and initial conformations are generated for polyampholyte. The number of the chains is $N_c = 6$, that of the monomers per chain is $N_1 = 32$, totaling the number of the monomers in the system $N = N_c N_1 = 192$. The charge sign of each monomer is chosen either positive or negative ($Z_i = \pm 1$) with the use of a random number. Thus, each chain has net charges δQ_α ($\alpha = 1 \sim N_c$), and the amount of global charge offset for one polyampholyte is expected to be $\delta Q = \sum_{\alpha=1}^{N_c} \delta Q_\alpha \sim e\sqrt{N}$ on average. As the boundary conditions, a reflecting sphere is placed at the radius $R = 21a$, as in Sec.3. To see bare behavior of non-neutral polyampholytes, counterions are not included in the present study.

The left column of Fig.9 shows, from top to bottom, the probability F of having the global charge offset δQ, which is nearly Gaussian centered at $\delta Q = 0$, the system gyration radius $R_{g,sys}$ which corresponds to the global size of polyampholyte, and the average gyration radius of the chains $R_{g,1}$. The bond-connected monomer distance d_{p-p}, the electrostatic energy W_p, and the filling index $\zeta = N_c^{1/3} R_{g,1}/R_{g.sys}$ are shown in the right column. Comparison of two kind of the gyration radii of Fig.9 reveals that the multichain effect depicted in $R_{g,sys}$ dominates in magnitude over the single-chain effect of $R_{g,1}$ in the swelling process of polyampholytes in solution. Repulsive Coulomb forces are apparent for highly non-neutral polyampholytes, as the connected monomer distances increase with the amount of global charge offset. The observation that the filling index becomes larger

than unity. $\zeta \geq 1$, for

$$\delta Q/Q \leq \frac{1}{2}\sqrt{N} \qquad (11)$$

($Q = eN$) indicates that we obtain a globule only for nearly neutral polyampholytes whose charge offset is given by Eq.(11). Otherwise, the charge complexes are disintegrated, and polyampholytes consist of non-overlapped scattered chains.

Figure 10 depicts the typical behavior of non-neutral polyampholytes in the heating stage that follows the cooling stage. The behavior in the heating stage is less deviated, as it starts from a compact globule. The deviations among the runs of different sequences but having the same value of global charge offset are small. The full width of the deviations in the gyration radii is equal or less than the symbol sizes, except for the mediumly charge offset cases, $\delta Q/Q \sim 6 - 8\%$ ($\cong N^{-1/2}$). For these intermediate cases with an interesting reentrant behavior (shown below), the full width of the deviations is roughly twice that of the symbol sizes. Even so, however, the overall profiles of changes are rather smooth and well preserved. The deviations for the filling index and electrostatic energy are as small as the symbol sizes.

The global charge offsets for the typical runs in Fig.10 are 0%, 5.2%, 6.3%, 8.3% and 12.5%. For the neutral case with $\delta Q = 0$, a globule is formed ($\zeta \geq 1$) for low temperatures $T/T_0 < 0.2$ (the Bjerrum length $\lambda_B > 5a$), as the electric dipole interactions between charge complexes are attractive. The system gyration radius increases monotonically with temperature. At high temperatures, polyampholyte reaches the thermal state in which the Coulomb forces play little role. This is the so-called *polyampholyte regime*[10,11].

For the very non-neutral case of $\delta Q/Q = 12.5\%$, the polyampholyte starts as an assembly of scattered chains at low temperatures due to electrostatic repulsions between excess charges. At high temperatures, chains come closer and the system gyration radius approaches that of the aforementioned thermal state (*the polyelectrolyte regime*). The chains are not overlapping ($\zeta < 1$) for non-neutral polyampholytes with the charge offset $\delta Q/Q > 1/2\sqrt{N}$, except for the polyampholyte with $\delta Q/Q \cong 1/\sqrt{N}$ at $T/T_0 \sim 0.2$. The electrostatic energy becomes less negative for larger charge offset, indicating less attractive nature of the Coulomb forces because of repulsions between the equal-sign charges.

It is remarkable that the system gyration radius for the medium charge offset cases ($\delta Q/Q \sim \sqrt{N}$) shows a reentrant behavior that has a minimum radius at intermediate temperatures. At this value of charge offset, the attractive force slightly overcomes the repulsive force. The system gyration radius first decreases with temperature, then turns to increase at certain temperatures. The temperature at which the system gyration radius is minimized shifts to the higher side when the charge offset becomes larger, which intensifies the repulsive forces, and broadens the polyelectrolyte regime.

The average gyration radius of individual chains behaves somewhat differently. For the polyampholytes with small charge offsets $\delta Q/Q < 10\%$, the radius $R_{g,1}$ increases monotonically with temperature. Only for a large charge offset case $\delta Q/Q \geq 10\%$, the average gyration radius becomes reentrant. This change is mostly attributed to the increase in the distance between the connected monomers d_{p-p}, which is suppressed in realistic polyampholytes with finite extensible chains.

Statistically averaged gyration radius $R_{g,sys}$ over the non-neutral polyampholytes of random sequences, whose case distribution was depicted in Fig.9, is shown with closed circles in Fig.11. For comparison, that for globally neutral polyampholytes is shown with open circles. This statistically averaged

gyration radius will indicate the swelling behavior of randomly co-polymerized polyampholyte (solution) that includes a large number of chains. As temperature is lowered, non-neutral polyampholyte shrinks, but less than the neutral one. Then, for the low temperatures $T/T_0 \leq 0.03$, they turn into a swelling phase. The statistically averaged behavior of the polyampholyte of random sequences is again reentrant, which resembles that of the non-neutral polyampholyte with $\delta Q/Q \sim 1/\sqrt{N}$.

(b) Simple mean-field theory

The swelling behavior of polyampholytes may be qualitatively understood by the following theoretical argument. As the multichain effects are dominating for the polyampholytes in solution, the elastic energy that mostly accounts for the single-chain effects may be neglected. The free energy is then approximated by

$$F = \frac{\delta Q^2}{\epsilon R_s} - \frac{e^3}{\epsilon^{3/2}T^{1/2}}\left(\frac{N}{R_s}\right)^{3/2} + \nu T \log\left(\frac{\nu}{V}\right). \quad (12)$$

In the equation, R_s is the system gyration radius of polyampholyte, δQ the excess charge, ν and N the number of chains and all charged monomers, respectively, and V the volume ($V \sim R_s^3$). The last term that accounts for the chain translational entropy appears only in the multichain system. The second term represents the attraction among the charge complexes. The first and third terms of Eq.(12) act to expand the polyampholyte, which decrease with the radius. The second term compresses polyampholyte, and increases with the radius.

If we take the fluctuations of each chain into account, the third term should be written as

$$F_1 = \nu T \log\left\{\nu\left(\frac{a}{R_s - R_1 + a}\right)^3\right\} + \nu T\left(\frac{R_1^2}{N_1 a^2} + \frac{N_1 a^2}{R_1^2}\right), \quad (13)$$

where R_1 and N_1 are the average gyration radius and the number of monomers of each chain, respectively. If we differentiate the free energy by R_1, we have

$$\frac{\partial F}{\partial R_1} = \nu T\left\{\frac{3}{R_s - R_1 + a} + \frac{2R_1}{N_1 a^2} - \frac{2N_1 a^2}{R_1^3}\right\}. \quad (14)$$

Then, for $R_s \gg R_1$, we have the Gaussian chains, $R_1 \sim aN_1^{1/2}$. In the other limit with $R_s \sim R_1$, we have $R_1 \sim R_s(1 - R_s^2/N_1 a^2)$.

To obtain the global shape, we differentiate the free energy with respect to the system gyration radius R_s and equate it with zero,

$$\frac{\partial F}{\partial R_s} = -\frac{\delta Q^2}{\epsilon R_s^2} + \frac{3}{2}\frac{e^3 N^{3/2}}{\epsilon^{3/2}T^{1/2}R_s^{5/2}} - \frac{3\nu T}{R_s} = 0. \quad (15)$$

For neutral polyampholyte ($\delta Q = 0$), the free energy takes a maximum value at the critical radius $R_c = (2\nu)^{-2/3}e^2 N/\epsilon T = (2\nu)^{-2/3}Na\Gamma$. Segregated phase with a globule and one-phase state with homogeneously scattered chains are separated at this radius $R_s = R_c$. The radius of the one-phase state for $R_s > R_c$ is not bound, whereas the radius for $R_s < R_c$ is limited by the volume exclusion effect. The increase in temperature makes the critical radius decrease, which causes more polyampholyte chains to reside in the swollen regime. This means that neutral polyampholyte is collapsed at low temperatures and swells up monotonically with the increase in temperature.

For the case of small excess charges, we set $R_s = R_c + \delta R$ and solve Eq.(15) for small δR. Then, one has a negative value $\delta R \sim -\frac{2}{15}\delta Q^2/\epsilon\nu T < 0$, the magnitude of which decreases with temperature. Numerical solution of the equation yields much smaller value

R_c for non-neutral polyampholytes than for neutral ones. That is, non-neutral polyampholyte is swollen at low temperatures and shrinks with the increase in temperature. Also, non-neutral polyampholyte is generally more swollen than its neutral counterpart, since $\delta R_s < 0$ for $\delta Q \neq 0$. However, Eq.(12) does not reproduce the reentrant behavior, which might require internal rearrangements of the chains and monomers.

(c) Comparison with experiments

There are experiments that measured the volumetric changes of polyampholyte polymers and gels against salt concentration[9–11]. In these experiments, it was shown that the volume of charge-balanced and highly charge-unbalanced polyampholytes, respectively, increased and decreased monotonically with the salt concentration. For mediumly unbalanced cases, the volume first decreased and then increased with addition of salt. The volumes of polyampholytes having different charge offsets reached almost a similar value at high salt concentration ($C_s \geq 0.1$ mol/l).

On the other hand, temperature is more easily changed in molecular dynamic simulations, as shown in this paper, without significant increase in the computation time. We note that, even if salt and temperature act differently on polyampholytes, salt ionic strength and temperature cause similar effects in the sense that the salt density n_s and temperature T both appear in the denominator of the electrostatic coupling constant, $\Gamma = (e^2/\epsilon a k_B T)(n_0/Z_s^2 n_s) \sim 1/n_s T$ (see Sec.1).

When we replace the salt concentration for the experiments with the temperature for the simulations on the horizontal axes, we find very good agreements of the results between our molecular dynamics simulation (Fig.10) and the experiments. One difference is that the transition from *the polyampholyte regime* (monotonic volume increase upon heating or salt addition) to *the polyelectrolyte regime* (monotonic volume decrease upon heating) occurs at a significantly smaller charge offset in the molecular dynamics simulations than in the experiments. This is quite possibly attributed to counterions: the present simulation system does not include neutralizing counterions, whereas in the experiments excess charges are always buffered by counterions. It is conjectured that the net excess charge in the experiments is by an order of magnitude smaller than the expected (labeled) amount, due to the shielding effects by counterions.

5. Summary

In this paper, we studied the condensation and swelling behavior of *multichain* polyampholytes with the use of molecular dynamics simulations. We focused on the temperature effects of very wide range, which is parallel to the salt ionic strength (See Sec.1). It was shown that the multichain effect predominates for the polyampholytes in solution. Obviously, the chain connection between charged monomers made condensation of polyampholytes faster than the free charged particles (plasma).

We showed that the complexes of positively and negatively charged monomers are formed, which made the Coulomb forces attractive. The neutral polyampholyte collapsed to a globule at low temperatures, in which the polymer chains inter-penetrated with each other and reptated through the whole volume of the globule. At high temperatures, neutral polyampholyte swelled monotonically to the thermal state, in which thermal motion of monomers prevails and the Coulomb forces play no role. This corresponded to a polyampholyte regime where the Coulomb forces are of attractive nature.

Hysteresis occurred in the global volume of polyampholyte, which revealed that the globule is not thermally equilibrated even at low

temperatures as its relaxation time is very slow. The multichain effect always caused much larger swelling of polyampholyte than the single-chain effect did for both neutral and non-neutral cases, due to creation of large void space among the chains.

Condensation took place when temperature was extremely lowered. The state thus reached was shown to have an ordered structure close to the NaCl crystal. However, when finite extensible bonds and impenetrable monomers were adopted, the discrete structure was not complete and frustrations were retained in the condensed globule.

Swelling behavior of non-neutral polyampholyte was also examined. It was shown that a globule is obtained only for a small charge offset $\delta Q < (1/2)N^{1/2}$; otherwise, non-neutral polyampholyte was swollen at low temperatures due to Coulomb repulsions between excess charges (polyelectrolyte regime). This shrank to the volume of the thermal (non-Coulombic) state at high temperature. Slightly non-neutral polyampholyte showed a reentrant behavior: it behaved as polyelectrolyte and polyampholyte at low and high temperatures, respectively.

These simulation results for non-neutral polyampholytes in the temperature domain were in very good agreements with the polyampholytic polymer and gel experiments that varied salt concentrations. Mean-field theory with the free energy that included repulsive and attractive electrostatic terms and translational term explained the swelling behavior of polyampholytes in the polyelectrolyte and polyampholyte regimes. But, one needed to include internal rearrangements of charged monomers to reproduce the reentrant behavior of the polyampholyte with a slightly charge offset.

Acknowledgments

One of the authors (M.T.) is very grateful to Prof.I.Ohmine for discussion of the crystal formation, and Prof. S.J. Candau for informations of his polyampholytic gel experiments. He also appreciates fruitful discussions with Prof.J.F.Joanny, Prof.F.Candau, Prof.K.Kremer, and Dr.C.Holm.

References

1. F.Candau and J.-F.Joanny, *Encyclopedia of Polymeric Materials*, edited by J.C.Salomone (CRC, Boca Raton, 1996), vol.7, pg.5476.
2. P.G.Higgs and J.-F.Joanny, J.Chem.Phys., 94, 1543 (1990).
3. A.V.Dobrynin and M.Rubinstein, J.Phys., II 5, 677 (1994).
4. Y.Kantor, M.Kardar, and H.Li, Phys.Rev., E 49, 1383 (1994).
5. R.Everaers, A.Johner and J.-F.Joanny, Europhys.Lett., 37, 275 (1997).
6. M.Tanaka, A.Yu Grosberg, V.S.Pande, and T.Tanaka, Phys.Rev., E 56, 5798 (1997)
7. M.Tanaka, A.Yu Grosberg, and T.Tanaka, J.Chem.Phys., 110, 8176 (1999).
8. T. Soddemann, H. Shiessel and A. Blumen, Phys.Rev., E 57, 2081 (1998).
9. J.M.Corpart and F.Candau, Macromolec. 26, 1333 (1993).
10. A.E.English, S.Mafe, J.A.Manzanares, X.H.Yu, A.Yu Grosberg, and T.Tanaka, J.Chem.Phys., 104, 8713 (1996).
11. G.Nisato, J.-P.Munich and S.J.Candau, Langmuir, 15, 4236 (1999).
12. M.Tanaka, A.Yu Grosberg, and T.Tanaka, *Slow Dynamics in Complex Systems*, p.599 (edited by M.Tokuyama and I.Oppenheim, AIP Conference Series, 1999).
13. M.Deserno and C.Holm, J.Chem.Phys., 109, 7678 (1998).
14. P-G. de Gennes, *Scaling Concepts in Polymer Physics* (Cornell Univ. Press, Ithaca, 1979).

Table and Caption

Table I. The charge sequences are listed for the globally neutral polyampholytes shown in Fig.1 and 3, and for the non-neutral polyampholyte in Fig.10 (the case of charge offset $\delta Q/Q = 8.3\%$). Each run uses six 32-mer chains, as numbered from (1) to (6) below; + and − represent positive and negative monomers, respectively, and the rightmost value shows local charge offset of each chain. The charge sequences are all at random, except for the global charge neutrality constraint in the cases of Fig.1 and 3.

Fig.1: $\delta Q/Q = 0$.

(1) − − + + + − + + + − + − + + − − + − − + + − − − − − + − + − -4.

(2) − − + − + − + + − − − − + + + − + − + + − − − + + + − − − − -6.

(3) + − + − + + + − + − − − + + + − − + − + − + − + − + − + − + − 0.

(4) − + + − + − + − + − + − − + + + + + − + − + − − − + + + − + − +2.

(5) + − + + + − − − + − − − + − + + + + − − + + + − + + + − + − + − +4.

(6) + − + + + − + − − − − + − + − + − + − + + + + + + + + − + − − + +4.

Fig.2: $\delta Q/Q = 0$.

(1) − − − − − − − − + − + − + − + + + + + + + − + + + + + + + − − − 0.

(2) − + − − − + + + + + − − + + + + + − − − + − + − + − − − − + − 0.

(3) + − + − + − − + + + + − − + − + + + − + + + − + − − − + + + − + − +2.

(4) − − − + + − + − + + − − − − + − − + + − + + − − − + + + − − + -4.

(5) − − + − + + − − + + − + + − + − − + + − − − − − − − + + + + + − -2.

(6) + − + + − − + + + + + + + − − − + + − + + + − + + + + + + − − + − +4.

Fig.9: $\delta Q/Q = 8.3\%$

(1) − − − + + + + + + − + + + + − + − + − + − − + + − + + + − + + − − +4.

(2) + + + + + + − − + + − + + + − + − + + + + − + − + − + − + + − + + +14.

(3) − + + − + + + − + − − + + − + − − − − − − − − + + + + − − − + + + − − -6.

(4) + − − − + − + + + − − − + − + + + + + + − + − + + + + + − + + − + +4.

(5) + − + + + + − − − − − − + + − + − + − + + + + + + + + + − − − − −2.

(6) − − + − − + − − + − − − + + + − − + − − − + + + + + + − + − + + -2.

Figure Captions

Figure 1. The behavior of globally neutral polyampholyte that consists of six 32-mer chains is shown for the cooling and (subsequent) heating stages with closed and open circles, respectively. The time constant of temperature changes is $\tau_g = 2000\omega_p^{-1}$. The system gyration radius of all the monomers $R_{g,sys}$, the average gyration radius of the chains $R_{g,1}$, the filling index that indicates overlap of the chains $\zeta = N_c^{1/3} R_{g,1}/R_{g,sys}$, the electrostatic energy $-W_p$ (sign reversed), the average distance of connected monomers d_{p-p}, and time fluctuations of the monomer distances δR, are shown against temperature T; T_0 is the base temperature for which the magnitude of the electrostatic and thermal energies are equalled.

Figure 2. The behavior of plasma (charged particles) with overall charge neutrality is shown for the cooling and heating stages with filled and open circles, respectively. The system gyration radius $R_{g,sys}$, and the electrostatic energy $-W_p$ (sign reversed) are shown against temperature T.

Figure 3. The effect of chain bonds on polyampholytes is depicted as the difference between a plasma in the heating stage (triangles) and a globally neutral polyampholyte in the cooling (closed circles) and heating (open circles) stages. The time constant of temperature changes is $\tau_g = 2000\omega_p^{-1}$. The system gyration radius of all the monomers $R_{g,sys}$, the average gyration radius of the chains $R_{g,1}$, the filling index that indicates overlap of the chains $\zeta = N_c^{1/3} R_{g,1}/R_{g,sys}$, the electrostatic energy $-W_p$ (sign reversed, $W_p = (1/N) \sum_{i>j} Z_i Z_j e^2/\epsilon |\mathbf{r}_i - \mathbf{r}_j|$), are shown against temperature T. Deviations from those in Fig.1 are due to different sequences and initial conformation.

Figure 4. Bird's-eye view of an NaCl-like crystal that is obtained for the globally neutral polyampholyte of Fig.3, at temperature $T/T_0 = 1/512$ in the cooling stage. The red and green spheres represent positively and negatively charged monomers, respectively. View angles are about 90 degrees different between the upper and lower frames.

Figure 5. Time evolution of the neutral polyampholyte in the cooling stage of Fig.3 is shown with the bird's-eye view plots (left) and the pair correlation functions (right). The four frames from top to bottom, respectively, correspond to temperatures $T/T_0 = 1/8$, $1/32$, $1/128$ and $1/512$. The $+$ and $\circ$ in the left column represent positive and negative monomers, respectively, and $G_{++}(r)$ and $G_{+-}(r)$ are the pair correlation

Figure 6. The combined effect of inextensible chains and impenetrable chains is shown for the globally neutral polyampholyte, for which the bond length is limited by $|\mathbf{r}_i - \mathbf{r}_{i+1}| \leq r_{max} = 1.4a$. The time constant of temperature changes is $\tau_g = 2000\omega_p^{-1}$. The system gyration radius $R_{g,sys}$, the average gyration radius of the chains $R_{g,1}$, the filling index $\zeta = N_c^{1/3} R_{g,1}/R_{g,sys}$, the electrostatic energy $-W_p$ (sign reversed), the average distance of connected monomers d_{p-p}, and mean-square fluctuation of the monomer distances δR, are shown against temperature T.

Figure 7. The condensed globule that is obtained for the neutral polyampholyte with inextensible chains of Fig.6, at temperature $T/T_0 = 1/512$ in the cooling stage. The red and green spheres represent positively and negatively charged monomers, respectively.

Figure 8. The bird's-eye view plot (left) and the pair correlation functions (right) for the polyampholyte with inextensible chains of Fig.6, at temperature $T/T_0 = 1/512$. The $G_{++}(r)$ and $G_{+-}(r)$ pair correlation functions are averages for the pairs of equal-sign and opposite-sign charges, respectively.

Figure 9. The effect of charge offset on non-neutral polyampholytes are depicted for 180 cases of six 32-mer chains of random sequences. The probability F of having global charge offset δQ, the system gyration radius $R_{g,sys}$, the average gyration radius of the chains $R_{g,1}$, the average distance between connected monomers d_{p-p}, the electrostatic energy W_p, and the filling index $\zeta = N_c R_{g,1}/R_{g,sys}$ are shown against charge offset at temperature $T/T_0 = 1/640$. The global charge offset of polyampholytes in the horizontal axis is normalized by the number of charged monomers, $Q = eN$.

Figure 10. Typical behaviors of globally non-neutral polyampholytes in the heating stage are shown against temperature: the system gyration radius $R_{g,sys}$, the average gyration radius of the chains $R_{g,1}$, the filing index $\zeta = N_c^{1/3} R_{g,1}/R_{g,sys}$, and the electrostatic energy W_p. Filled and open circles, filled and open triangles, and squares correspond to the global charge offsets of $\delta Q/Q = 0.0\%$, 5.2%, 6.3%, 8.3% and 12.5%, respectively.

Figure 11. The swelling behavior of statistically averaged system gyration radius $R_{g,sys}$, and the gyration radius of each chain $R_{g,1}$. The average is taken over 180 non-neutral polyampholytes of random sequences of Fig.9.

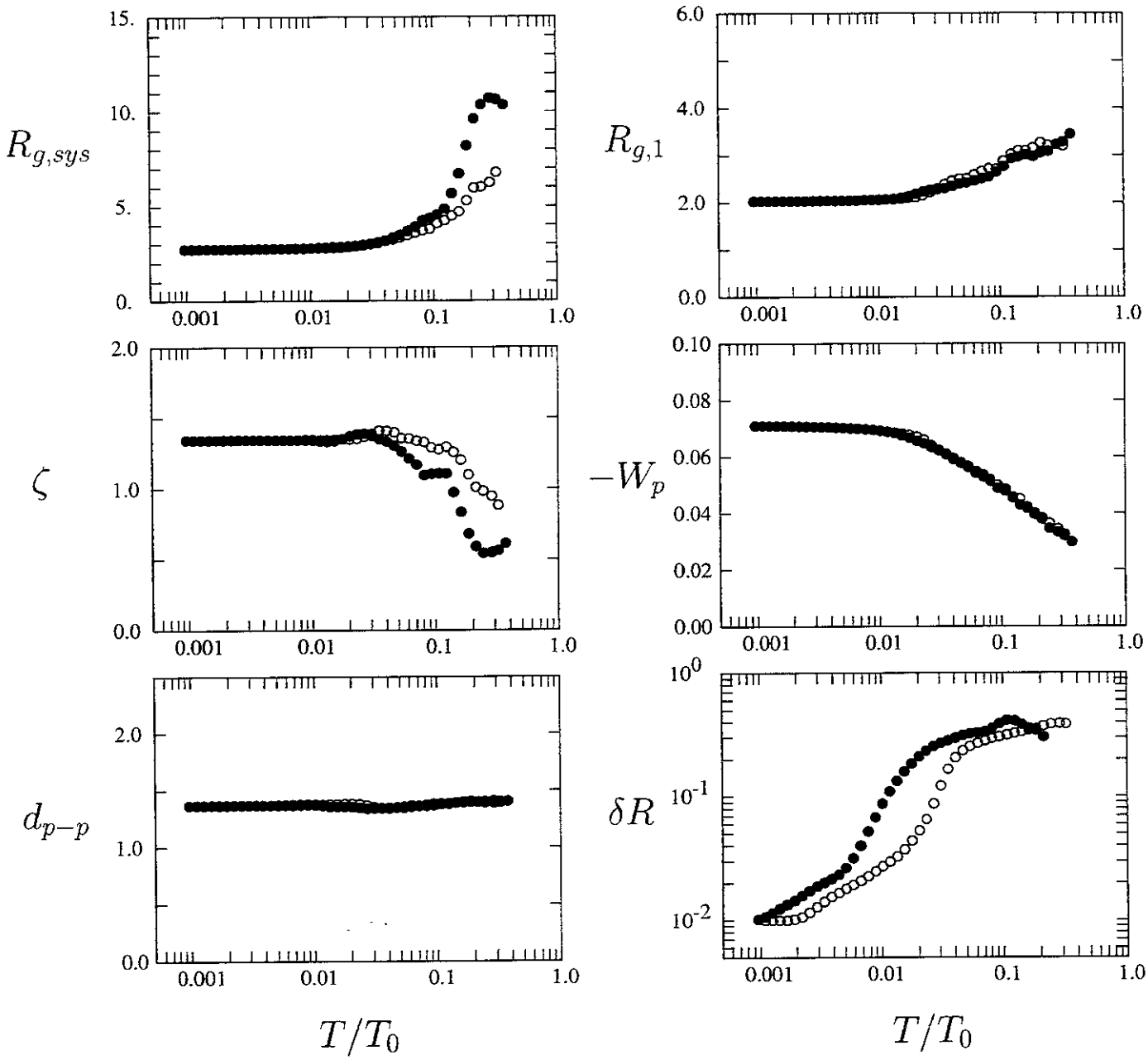
$R_{g,sys}$
15.
10.
5.
0.
0.001
0.01
0.1
1.0
$R_{g,1}$
6.0
4.0
2.0
0.0
ζ
2.0
1.0
0.0
$-W_p$
0.10
0.08
0.06
0.04
0.02
0.00
d_{p-p}
δR
10^0
10^{-1}
10^{-2}
T/T_0

Figure 1

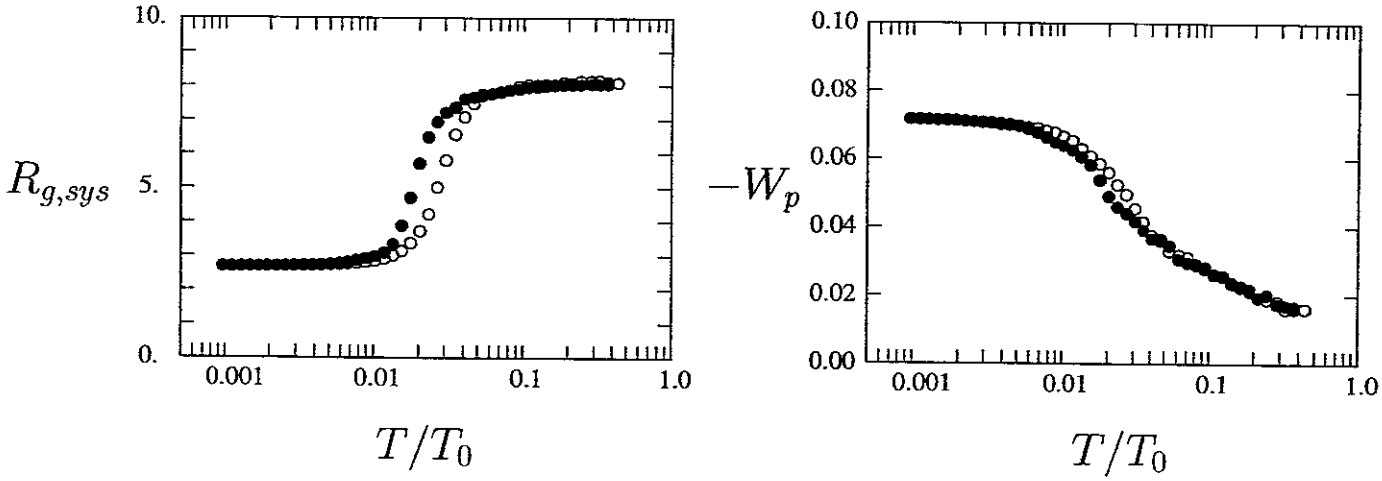

Figure 2

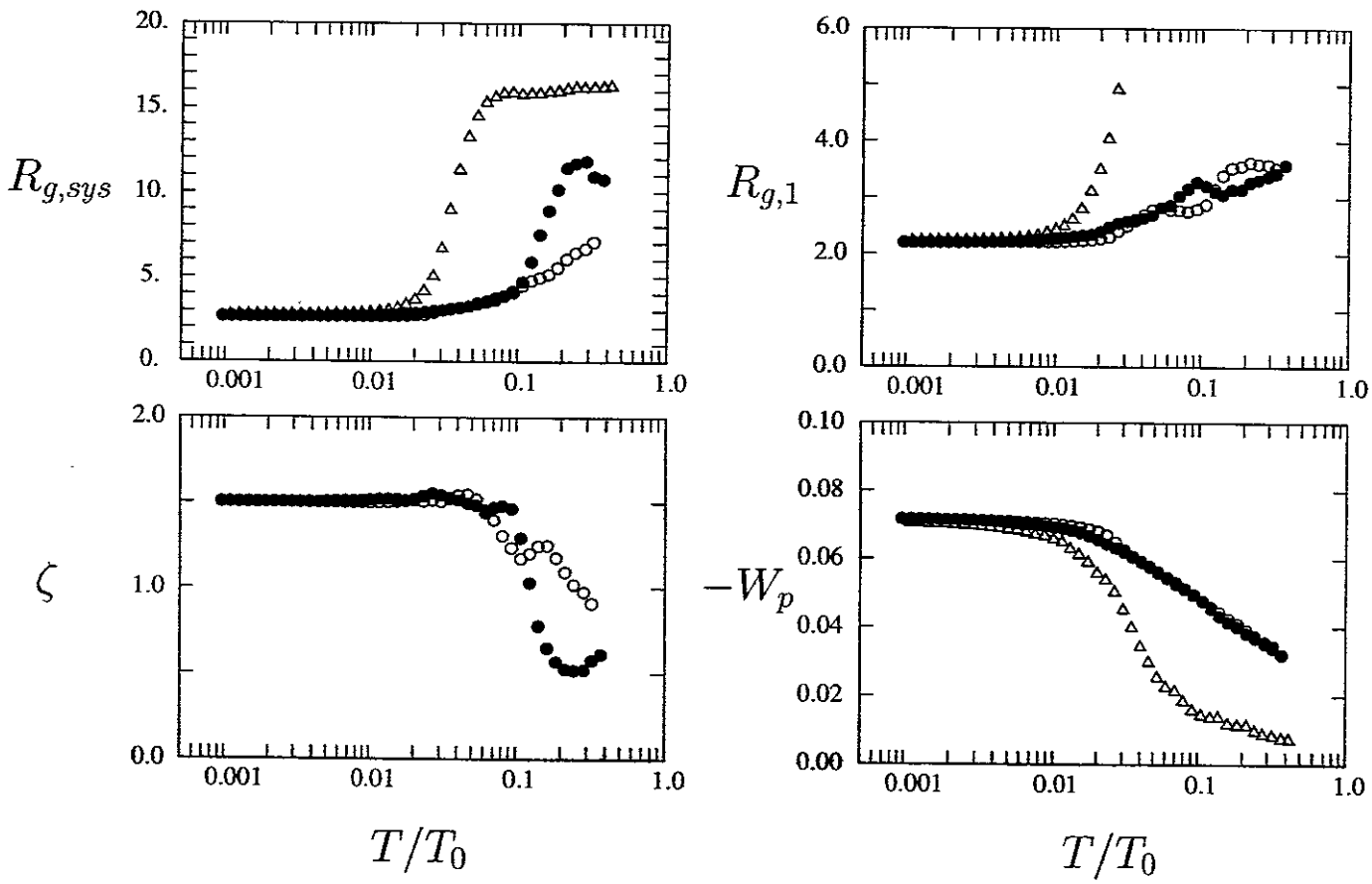

Figure 3

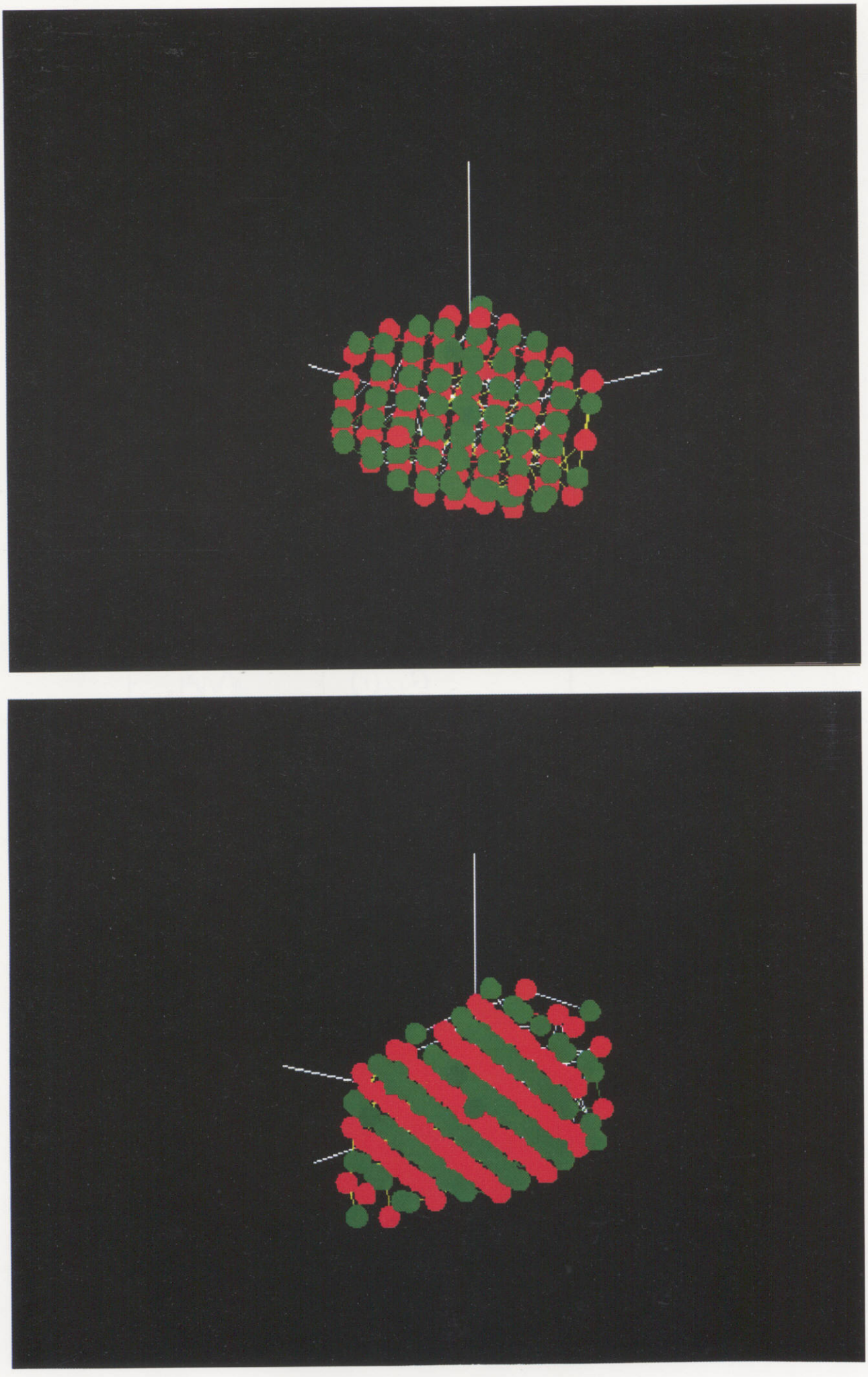

Figure 4.

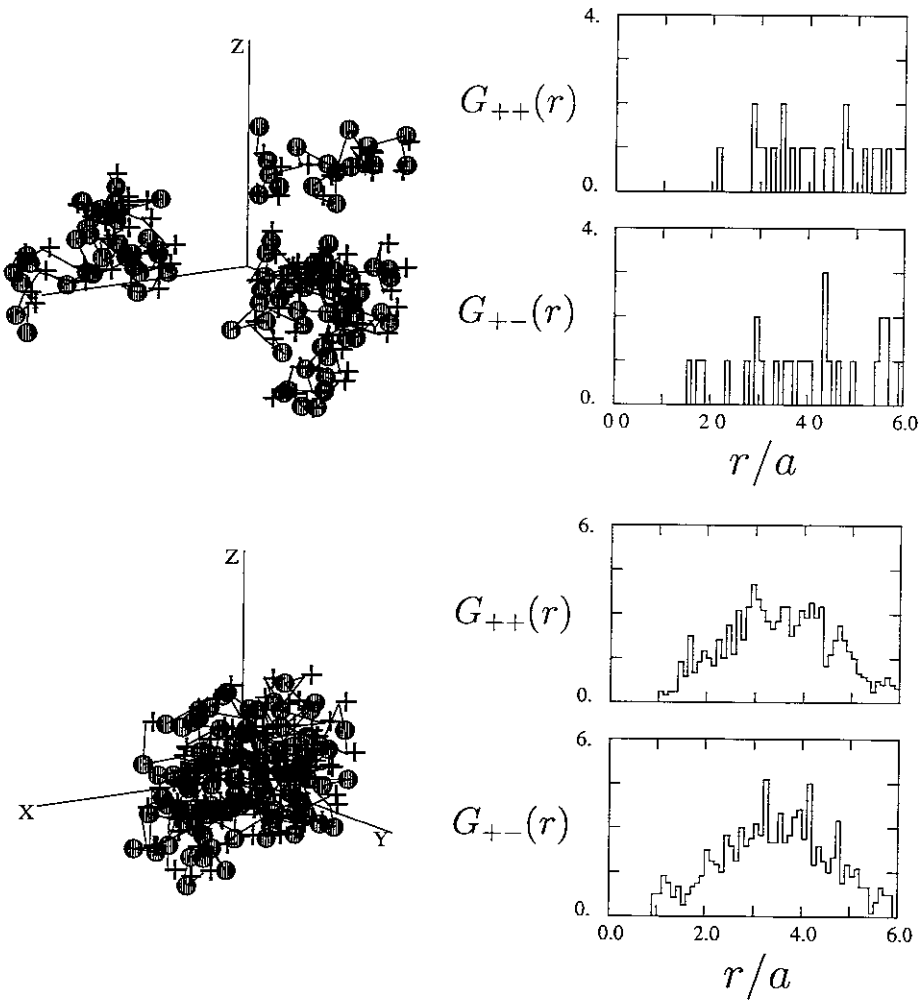

Figure 5a

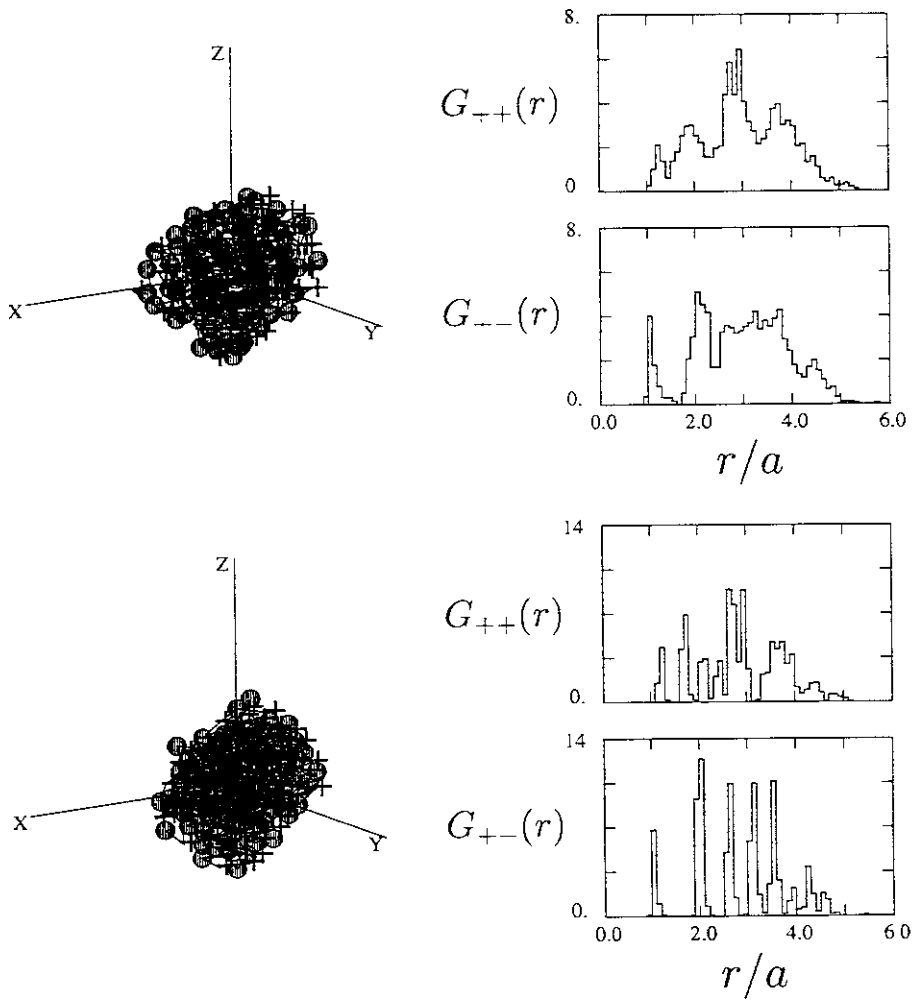

Figure 5b

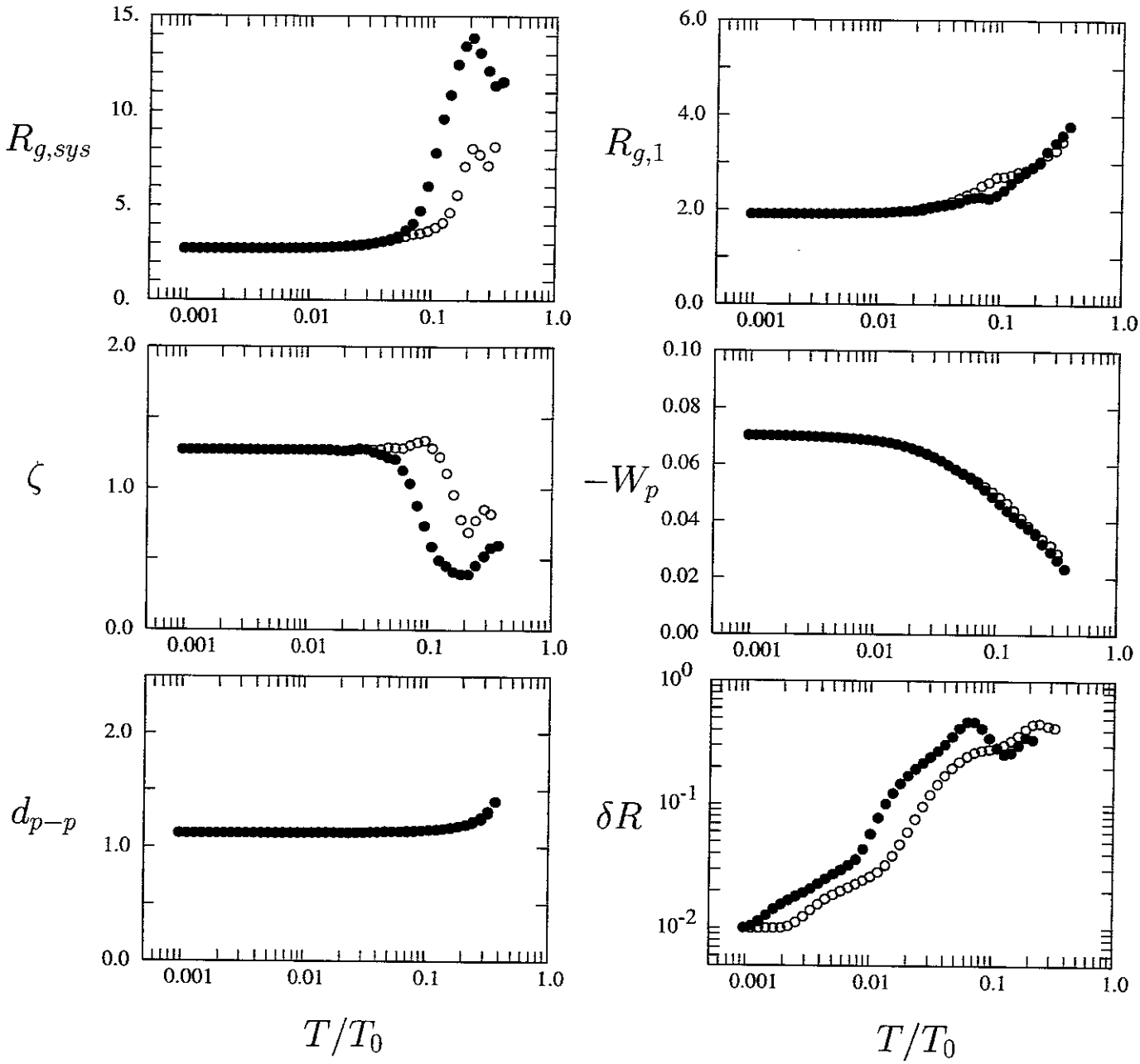

Figure 6

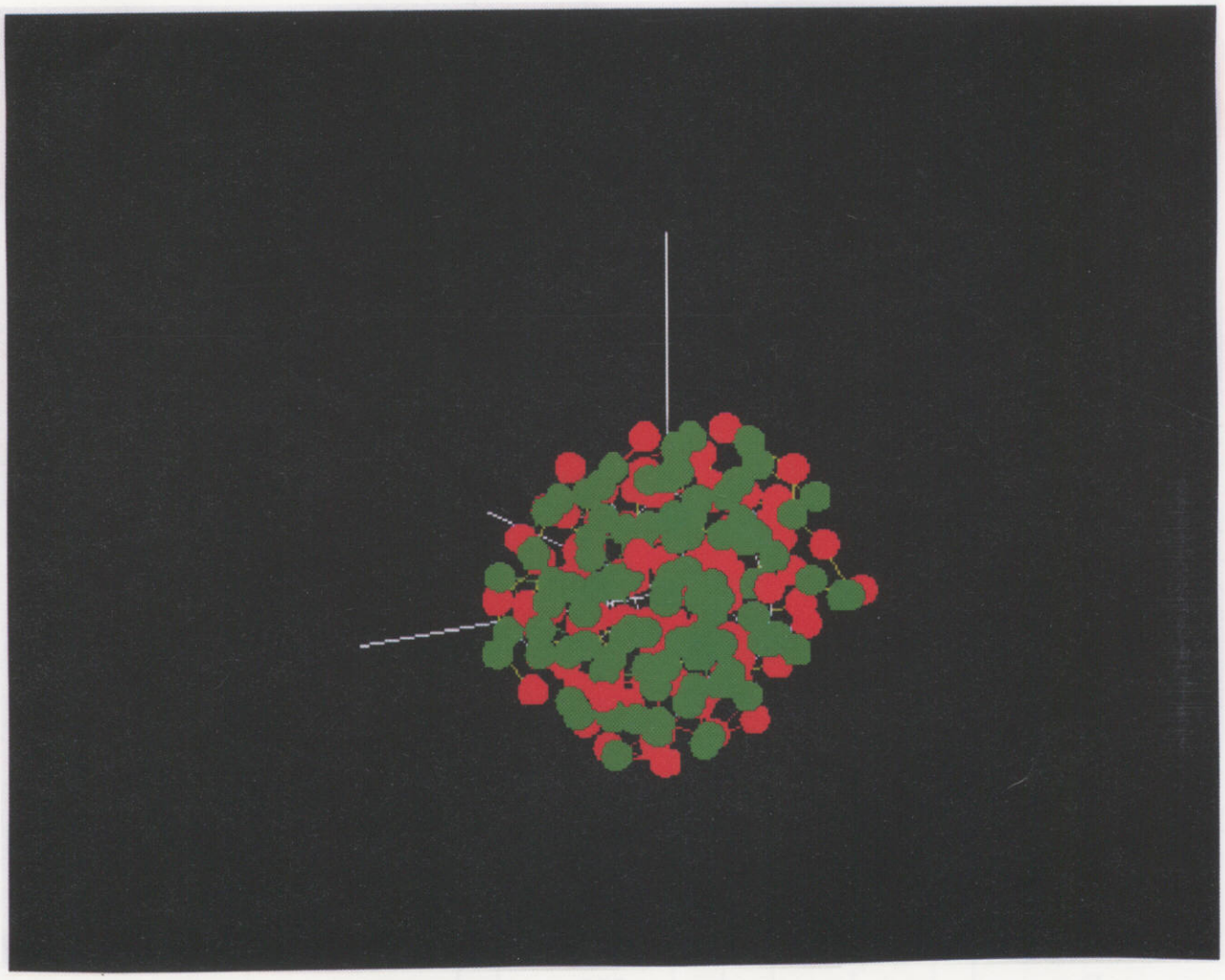

Figure 7.

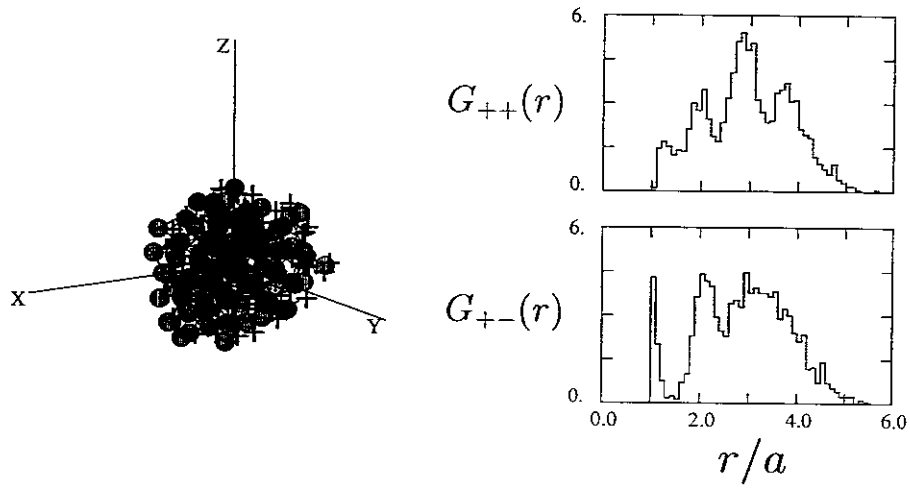

Figure 8

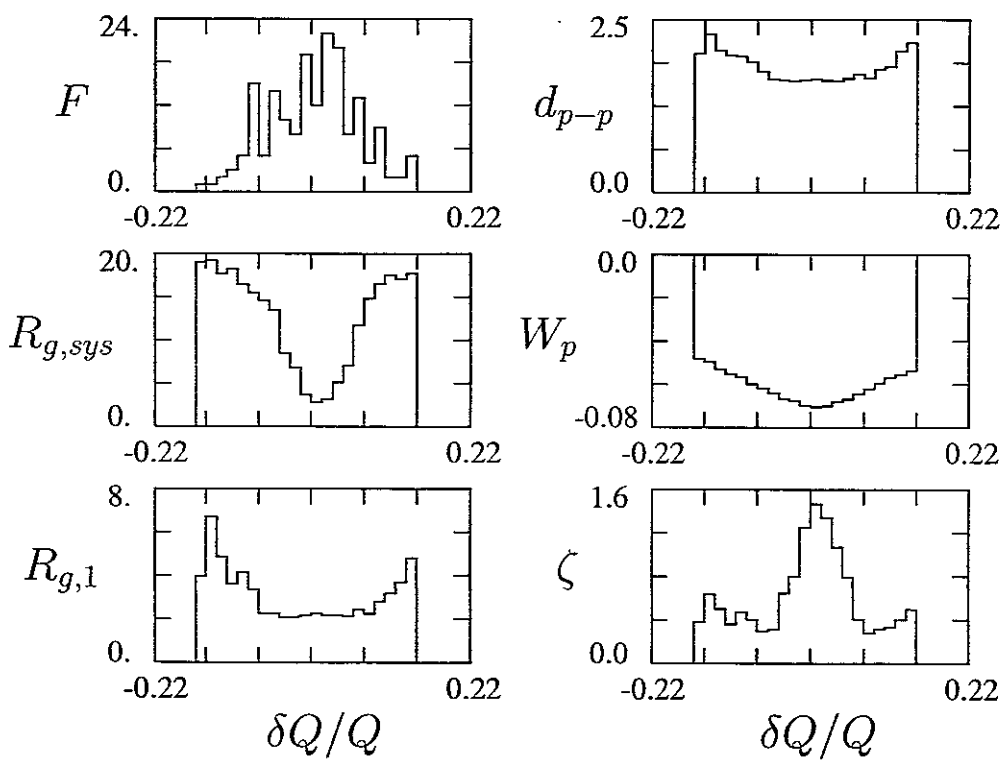

Figure 9

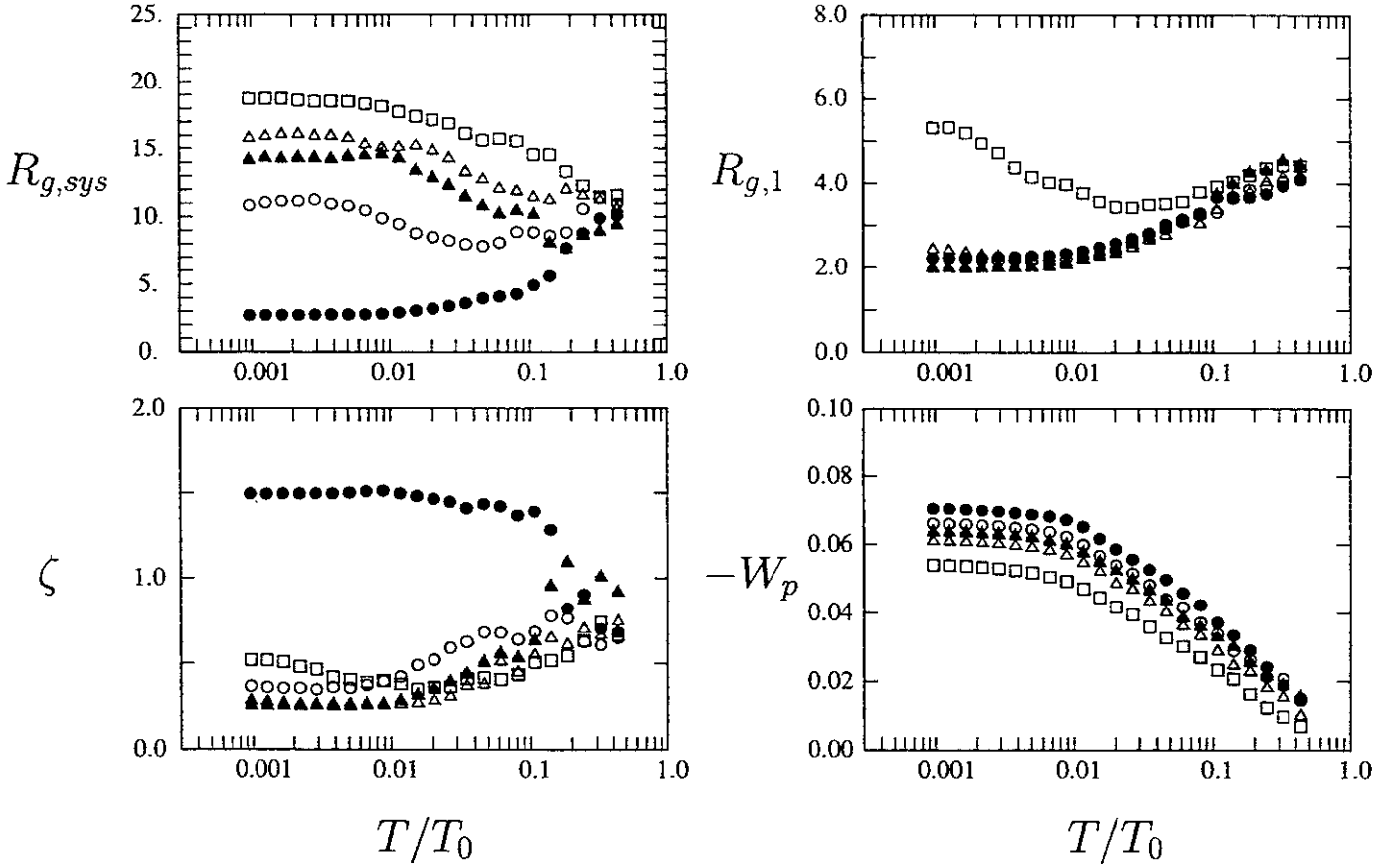

Figure 10

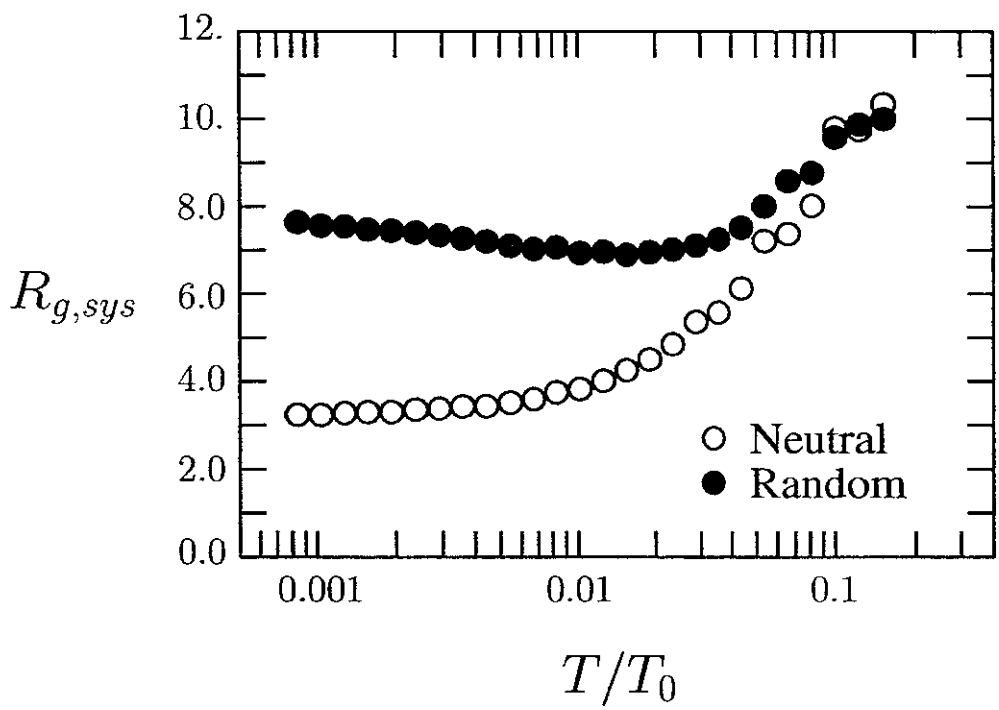

Figure 11.

Recent Issues of NIFS Series

NIFS-553 N. Noda, K. Tsuzuki, A. Sagara, N. Inoue, T. Muroga,
oronaization in Future Devices -Protecting Layer against Tritium and Energetic Neutrals-: July 1998

NIFS-554 S. Murakami and H. Saleem,
Electromagnetic Effects on Rippling Instability and Tokamak Edge Fluctuations; July 1998

NIFS-555 H. Nakamura , K. Ikeda and S. Yamaguchi,
Physical Model of Nernst Element; Aug. 1998

NIFS-556 H. Okumura, S. Yamaguchi, H. Nakamura, K. Ikeda and K. Sawada,
Numerical Computation of Thermoelectric and Thermomagnetic Effects; Aug. 1998

NIFS-557 Y. Takeiri, M. Osakabe, K. Tsumori, Y. Oka, O. Kaneko, E. Asano, T. Kawamoto, R. Akiyama and M. Tanaka,
Development of a High-Current Hydrogen-Negative Ion Source for LHD-NBI System; Aug.1998

NIFS-558 M. Tanaka, A. Yu Grosberg and T. Tanaka,
Molecular Dynamics of Structure Organization of Polyampholytes; Sep. 1998

NIFS-559 R. Horiuchi, K. Nishimura and T. Watanabe,
Kinetic Stabilization of Tilt Disruption in Field-Reversed Configurations; Sep. 1998
(IAEA-CN-69/THP1/11)

NIFS-560 S. Sudo, K. Kholopenkov, K. Matsuoka, S. Okamura, C. Takahashi, R. Akiyama, A. Fujisawa, K. Ida, H. Idei, H. Iguchi, M. Isobe, S. Kado, K. Kondo, S. Kubo, H. Kuramoto, T. Minami, S. Morita, S. Nishimura, M. Osakabe, M. Sasao, B. Peterson, K. Tanaka, K. Toi and Y. Yoshimura,
Particle Transport Study with Tracer-Encapsulated Solid Pellet Injection; Oct. 1998
(IAEA-CN-69/EXP1/18)

NIFS-561 A. Fujisawa, H. Iguchi, S. Lee, K. Tanaka, T. Minami, Y. Yoshimura, M. Osakabe, K. Matsuoka, S. Okamura, H. Idei, S. Kubo, S. Ohdachi, S. Morita, R. Akiyama, K. Toi, H. Sanuki, K. Itoh, K. Ida, A. Shimizu, S. Takagi, C. Takahashi, M. Kojima, S. Hidekuma, S. Nishimura, M. Isobe, A. Ejiri, N. Inoue, R. Sakamoto, Y. Hamada and M. Fujiwara,
Dynamic Behavior Associated with Electric Field Transitions in CHS Heliotron/Torsatron; Oct. 1998
(IAEA-CN-69/EX5/1)

NIFS-562 S. Yoshikawa,
Next Generation Toroidal Devices; Oct. 1998

NIFS-563 Y. Todo and T. Sato,
Kinetic-Magnetohydrodynamic Simulation Study of Fast Ions and Toroidal Alfvén Eigenmodes; Oct. 1998
(IAEA-CN-69/THP2/22)

NIFS-564 T. Watari, T. Shimozuma, Y. Takeiri, R. Kumazawa, T. Mutoh, M. Sato, O. Kaneko, K. Ohkubo, S. Kubo, H. Idei, Y. Oka, M. Osakabe, T. Seki, K. Tsumori, Y. Yoshimura, R. Akiyama, T. Kawamoto, S. Kobayashi, F. Shimpo, Y. Takita, E. Asano, S. Itoh, G. Nomura, T. Ido, M. Hamabe, M. Fujiwara, A. Iiyoshi, S. Morimoto, T. Bigelow and Y.P. Zhao,
Steady State Heating Technology Development for LHD: Oct. 1998
(IAEA-CN-69/FTP/21)

NIFS-565 A. Sagara, K.Y. Watanabe, K. Yamazaki, O. Motojima, M. Fujiwara, O. Mitarai, S. Imagawa, H. Yamanishi, H. Chikaraishi, A. Kohyama, H. Matsui, T. Muroga, T. Noda, N. Ohyabu, T. Satow, A.A. Shishkin, S. Tanaka, T. Terai and T. Uda,
LHD-Type Compact Helical Reactors; Oct. 1998
(IAEA-CN-69/FTP/03(R)

NIFS-566 N. Nakajima, J. Chen, K. Ichiguchi and M. Okamoto,
Global Mode Analysis of Ideal MHD Modes in L=2 Heliotron/Torsatron Systems; Oct. 1998
(IAEA-CN-69/THP1/08)

NIFS-567 K. Ida, M. Osakabe, K. Tanaka, T. Minami, S. Nishimura, S. Okamura, A. Fujisawa, Y. Yoshimura, S. Kubo, R. Akiyama, D.S.Darrow, H. Idei, H. Iguchi, M. Isobe, S. Kado, T. Kondo, S. Lee, K. Matsuoka, S. Morita, I. Nomura, S. Ohdachi, M. Sasao, A. Shimizu, K. Tumori, S. Takayama, M. Takechi, S. Takagi, C. Takahashi, K. Toi and T. Watari,
Transition from L Mode to High Ion Temperature Mode in CHS Heliotron/Torsatron Plasmas; Oct. 1998
(IAEA-CN-69/EX2/2)

NIFS-568 S. Okamura, K. Matsuoka, R. Akiyama, D.S. Darrow, A. Ejiri, A. Fujisawa, M. Fujiwara, M. Goto, K. Ida H. Idei, H. Iguchi, N. Inoue, M. Isobe, K. Itoh, S. Kado, K. Khlopenkov, T. Kondo, S. Kubo, A. Lazaros, S. Lee, G. Matsunaga, T. Minami, S. Morita, S. Murakami, N. Nakajima, N. Nikai, S. Nishimura, I. Nomura, S. Ohdachi, K. Ohkuni, M. Osakabe, R. Pavlichenko, B. Peterson, R. Sakamoto, H. Sanuki, M. Sasao, A. Shimizu, Y. Shirai, S. Sudo, S. Takagi, C. Takahashi, S. Takayama, M. Takechi, K. Tanaka, K.

Toi, K. Yamazaki, Y. Yoshimura and T. Watari,
Confinement Physics Study in a Small Low-Aspect-Ratio Helical Device CHS;Oct. 1998
(IAEA-CN-69/OV4/5)

NIFS-569 M.M. Skoric, T. Sato, A. Maluckov, M.S. Jovanovic,
Micro- and Macro-scale Self-organization in a Dissipative Plasma;Oct. 1998

NIFS-570 T. Hayashi, N. Mizuguchi, T-H. Watanabe, T. Sato and the Complexity Simulation Group,
Nonlinear Simulations of Internal Reconnection Event in Spherical Tokamak;Oct. 1998
(IAEA-CN-69/TH3/3)

NIFS-571 A. Iiyoshi, A. Komori, A. Ejiri, M. Emoto, H. Funaba, M. Goto, K. Ida, H. Idei, S. Inagaki, S. Kado, O. Kaneko, K. Kawahata, S. Kubo, R. Kumazawa, S. Masuzaki, T. Minami, J. Miyazawa, T. Morisaki, S. Morita, S. Murakami, S. Muto, T. Muto, Y. Nagayama, Y. Nakamura, H. Nakanishi, K. Narihara, K. Nishimura, N. Noda, T. Kobuchi, S. Ohdachi, N. Ohyabu, Y. Oka, M. Osakabe, T. Ozaki, B.J. Peterson, A. Sagara, S. Sakakibara, R. Sakamoto, H. Sasao, M. Sasao, K. Sato, M. Sato, T. Seki, T. Shimozuma, M. Shoji, H. Suzuki, Y. Takeiri, K. Tanaka, K. Toi, T. Tokuzawa, K. Tsumori, I. Yamada, H. Yamada, S. Yamaguchi, M. Yokoyama, K.Y.Watanabe, T. Watari, R. Akiyama, H. Chikaraishi, K. Haba, S. Hamaguchi, S. Iima, S. Imagawa, N. Inoue, K. Iwamoto, S. Kitagawa, Y. Kubota, J. Kodaira, R. Maekawa, T. Mito. T. Nagasaka, A. Nishimura, Y. Takita, C. Takahashi, K. Takahata, K. Yamauchi, H. Tamura, T. Tsuzuki, S. Yamada, N. Yanagi, H. Yonezu, Y. Hamada, K. Matsuoka, K. Murai, K. Ohkubo, I. Ohtake, M. Okamoto, S. Sato, T. Satow, S. Sudo, S. Tanahashi, K. Yamazaki, M. Fujiwara and O. Motojima,
An Overview of the Large Helical Device Project; Oct. 1998
(IAEA-CN-69/OV1/4)

NIFS-572 M. Fujiwara, H. Yamada, A. Ejiri, M. Emoto, H. Funaba, M. Goto, K. Ida, H. Idei, S. Inagaki, S. Kado, O. Kaneko, K. Kawahata, A. Komori, S. Kubo, R. Kumazawa, S. Masuzaki, T. Minami, J. Miyazawa, T. Morisaki, S. Morita, S. Murakami, S. Muto, T. Muto, Y. Nagayama, Y. Nakamura, H. Nakanishi, K. Narihara, K. Nishimura, N. Noda, T. Kobuchi, S. Ohdachi, N. Ohyabu, Y. Oka, M. Osakabe, T. Ozaki, B. J. Peterson, A. Sagara, S. Sakakibara, R. Sakamoto, H. Sasao, M. Sasao, K. Sato, M. Sato, T. Seki, T. Shimozuma, M. Shoji, H. Sazuki, Y. Takeiri, K. Tanaka, K. Toi, T. Tokuzawa, K. Tsumori, I. Yamada, S. Yamaguchi, M. Yokoyama, K.Y. Watanabe, T. Watari, R. Akiyama, H. Chikaraishi, K. Haba, S. Hamaguchi, M. Iima, S. Imagawa, N. Inoue, K. Iwamoto, S. Kitagawa, Y. Kubota, J. Kodaira, R. Maekawa, T. Mito, T. Nagasaka, A. Nishimura, Y. Takita, C. Takahashi, K. Takahata, K. Yamauchi, H. Tamura, T. Tsuzuki, S. Yamada, N. Yanagi, H. Yonezu, Y. Hamada, K. Matsuoka, K. Murai, K. Ohkubo, I. Ohtake, M. Okamoto, S. Sato, T. Satow, S. Sudo, S. Tanahashi, K. Yamazaki, O. Motojima and A. Iiyoshi,
Plasma Confinement Studies in LHD; Oct. 1998
(IAEA-CN-69/EX2/3)

NIFS-573 O. Motojima, K. Akaishi, H. Chikaraishi, H. Funaba, S. Hamaguchi, S. Imagawa, S. Inagaki, N. Inoue, A. Iwamoto, S. Kitagawa, A. Komori, Y. Kubota, R. Maekawa, S. Masuzaki, T. Mito, J. Miyazawa, T. Morisaki, T. Muroga, T. Nagasaka, Y. Nakmura, A. Nishimura, K. Nishimura, N. Noda, N. Ohyabu, S. Sagara, S. Sakakibara, R. Sakamoto, S. Satoh, T. Satow, M. Shoji, H. Suzuki, K. Takahata, H. Tamura, K. Watanabe, H. Yamada, S. Yamada, S. Yamaguchi, K. Yamazaki, N. Yanagi, T. Baba, H. Hayashi, M. Iima, T. Inoue, S. Kato, T. Kato, T. Kondo, S. Moriuchi, H. Ogawa, I. Ohtake, K. Ooba, H. Sekiguchi, N. Suzuki, S. Takami, Y. Taniguchi, T. Tsuzuki, N. Yamamoto, K. Yasui, H. Yonezu, M. Fujiwara and A. Iiyoshi,
Progress Summary of LHD Engineering Design and Construction; Oct. 1998
(IAEA-CN-69/FT2/1)

NIFS-574 K. Toi, M. Takechi, S. Takagi, G. Matsunaga, M. Isobe, T. Kondo, M. Sasao, D.S. Darrow, K. Ohkuni, S. Ohdachi, R. Akiyama A. Fujisawa, M. Gotoh, H. Idei, K. Ida, H. Iguchi, S. Kado, M. Kojima, S. Kubo, S. Lee, K. Matsuoka, T. Minami, S. Morita, N. Nikai, S. Nishimura, S. Okamura, M. Osakabe, A. Shimizu, Y. Shirai, C. Takahashi, K. Tanaka, T. Watari and Y. Yoshimura,
Global MHD Modes Excited by Energetic Ions in Heliotron/Torsatron Plasmas;Oct. 1998
(IAEA-CN-69/EXP1/19)

NIFS-575 Y. Hamada, A. Nishizawa, Y. Kawasumi, A. Fujisawa, M. Kojima, K. Narihara, K. Ida, A. Ejiri, S. Ohdachi, K. Kawahata, K. Toi, K. Sato, T. Seki, H. Iguchi, K. Adachi, S. Hidekuma, S.Hirokura, K. Iwasaki, T. Ido, R. Kumazawa, H. Kuramoto, T. Minami, I.. Nomura, M. Sasao, K.N. Sato, T. Tsuzuki, I. Yamada and T. Watari,
Potential Turbulence in Tokamak Plasmas;Oct. 1998
(IAEA-CN-69/EXP2/14)

NIFS-576 S. Murakami, U. Gasparino, H. Idei, S. Kubo, H. Maassberg, N. Marushchenko, N. Nakajima, M. Romé and M. Okamoto,
5D Simulation Study of Suprathermal Electron Transport in Non-Axisymmetric Plasmas;Oct. 1998
(IAEA-CN-69/THP1/01)

NIFS-577 S. Fujiwara and T. Sato,
Molecular Dynamics Simulation of Structure Formation of Short Chain Molecules; Nov. 1998

NIFS-578 T. Yamagishi,
Eigenfunctions for Vlasov Equation in Multi-species Plasmas Nov. 1998

NIFS-579 M. Tanaka, A. Yu Grosberg and T. Tanaka,
Molecular Dynamics of Strongly-Coupled Multichain Coulomb Polymers in Pure and Salt Aqueous Solutions;Nov. 1998

NIFS-580 J. Chen, N. Nakajima and M. Okamoto,
Global Mode Analysis of Ideal MHD Modes in a Heliotron/Torsatron System: I. Mercier-unstable

Equilibria; Dec. 1998

NIFS-581 M. Tanaka, A. Yu Grosberg and T. Tanaka,
Comparison of Multichain Coulomb Polymers in Isolated and Periodic Systems: Molecular Dynamics Study; Jan. 1999

NIFS-582 V.S. Chan and S. Murakami,
Self-Consistent Electric Field Effect on Electron Transport of ECH Plasmas; Feb. 1999

NIFS-583 M. Yokoyama, N. Nakajima, M. Okamoto, Y. Nakamura and M. Wakatani,
Roles of Bumpy Field on Collisionless Particle Confinement in Helical-Axis Heliotrons; Feb. 1999

NIFS-584 T.-H. Watanabe, T. Hayashi, T. Sato, M. Yamada and H. Ji,
Modeling of Magnetic Island Formation in Magnetic Reconnection Experiment; Feb. 1999

NIFS-585 R. Kumazawa, T. Mutoh, T. Seki, F. Shinpo, G. Nomura, T. Ido, T. Watari, Jean-Marie Noterdaeme and Yangping Zhao,
Liquid Stub Tuner for Ion Cyclotron Heating; Mar. 1999

NIFS-586 A. Sagara, M. Iima, S. Inagaki, N. Inoue, H. Suzuki, K. Tsuzuki, S. Masuzaki, J. Miyazawa, S. Morita, Y. Nakamura, N. Noda, B. Peterson, S. Sakakibara, T. Shimozuma, H. Yamada, K. Akaishi, H. Chikaraishi, H. Funaba, O. Kaneko, K. Kawahata, A. Komori, N. Ohyabu, O. Motojima, LHD Exp. Group 1, LHD Exp. Group 2,
Wall Conditioning at the Starting Phase of LHD; Mar. 1999

NIFS-587 T. Nakamura and T. Yabe,
Cubic Interpolated Propagation Scheme for Solving the Hyper-Dimensional Vlasov-Poisson Equation in Phase Space; Mar. 1999

NIFS-588 W.X. Wnag, N. Nakajima, S. Murakami and M. Okamoto,
An Accurate δf Method for Neoclassical Transport Calculation; Mar. 1999

NIFS-589 K. Kishida, K. Araki, S. Kishiba and K. Suzuki,
Local or Nonlocal? Orthonormal Divergence-free Wavelet Analysis of Nonlinear Interactions in Turbulence; Mar. 1999

NIFS-590 K. Araki, K. Suzuki, K. Kishida and S. Kishiba,
Multiresolution Approximation of the Vector Fields on T^3; Mar. 1999

NIFS-591 K. Yamazaki, H. Yamada, K.Y.Watanabe, K. Nishimura, S. Yamaguchi, H. Nakanishi, A. Komori, H. Suzuki, T. Mito, H. Chikaraishi, K. Murai, O. Motojima and the LHD Group,
Overview of the Large Helical Device (LHD) Control System and Its First Operation; Apr. 1999

NIFS-592 T. Takahashi and Y. Nakao,
Thermonuclear Reactivity of D-T Fusion Plasma with Spin-Polarized Fuel; Apr. 1999

NIFS-593 H. Sugama,
Damping of Toroidal Ion Temperature Gradient Modes; Apr. 1999

NIFS-594 Xiaodong Li,
Analysis of Crowbar Action of High Voltage DC Power Supply in the LHD ICRF System; Apr. 1999

NIFS-595 K. Nishimura, R. Horiuchi and T. Sato,
Drift-kink Instability Induced by Beam Ions in Field-reversed Configurations; Apr. 1999

NIFS-596 Y. Suzuki, T-H. Watanabe, T. Sato and T. Hayashi,
Three-dimensional Simulation Study of Compact Toroid Plasmoid Injection into Magnetized Plasmas; Apr. 1999

NIFS-597 H. Sanuki, K. Itoh, M. Yokoyama, A. Fujisawa, K. Ida, S. Toda, S.-I. Itoh, M. Yagi and A. Fukuyama,
Possibility of Internal Transport Barrier Formation and Electric Field Bifurcation in LHD Plasma; May 1999

NIFS-598 S. Nakazawa, N. Nakajima, M. Okamoto and N. Ohyabu,
One Dimensional Simulation on Stability of Detached Plasma in a Tokamak Divertor; June 1999

NIFS-599 S. Murakami, N. Nakajima, M. Okamoto and J. Nhrenberg,

Effect of Energetic Ion Loss on ICRF Heating Efficiency and Energy Confinement Time in Heliotrons; June 1999

NIFS-600 R. Horiuchi and T. Sato,
Three-Dimensional Particle Simulation of Plasma Instabilities and Collisionless Reconnection in a Current Sheet;; June 1999

NIFS-601 W. Wang, M. Okamoto, N. Nakajima and S. Murakami,
Collisional Transport in a Plasma with Steep Gradients; June 1999

NIFS-602 T. Mutoh, R. Kumazawa, T. Saki, K. Saito, F. Simpo, G. Nomura, T. Watari, X. Jikang, G. Cattanei, H. Okada, K. Ohkubo, M. Sato, S. Kubo, T. Shimozuma, H. Idei, Y. Yoshimura, O. Kaneko, Y. Takeiri, M. Osakabe, Y. Oka, K. Tsumori, A. Komori, H. Yamada, K. Watanabe, S. Sakakibara, M. Shoji, R. Sakamoto, S. Inagaki, J. Miyazawa, S. Morita, K. Tanaka, B.J. Peterson, S. Murakami, T. Minami, S. Ohdachi, S. Kado, K. Narihara, H. Sasao, H. Suzuki, K. Kawahata, N. Ohyabu, Y. Nakamura, H. Funaba, S. Masuzaki, S. Muto, K. Sato, T. Morisaki, S. Sudo, Y. Nagayama, T. Watanabe, M. Sasao, K.. Ida, N. Noda, K. Yamazaki, K. Akaishi, A. Sagara, K. Nishimura, T. Ozaki, K. Toi, O. Motojima, M. Fujiwara, A. Iiyoshi and LHD Exp. Group 1 and 2,
First ICRF Heating Experiment in the Large Helical Device; July 1999

NIFS-603 P.C. de Vries, Y. Nagayama, K. Kawahata, S. Inagaki, H. Sasao and K. Nagasaki,
Polarization of Electron Cyclotron Emission Spectra in LHD; July 1999

NIFS-604 W. Wang, N. Nakajima, M. Okamoto and S. Murakami,
δf Simulation of Ion Neoclassical Transport; July 1999

NIFS-605 T. Hayashi, N. Mizuguchi, T. Sato and the Complexity Simulation Group,
Numerical Simulation of Internal Reconnection Event in Spherical Tokamak; July 1999

NIFS-606 M. Okamoto, N. Nakajima and W. Wang,
On the Two Weighting Scheme for δf Collisional Transport Simulation; Aug. 1999

NIFS-607 O. Motojima, A.A. Shishkin, S. Inagaki, K. Y. Watanabe,
Possible Control Scenario of Radial Electric Field by Loss-Cone-Particle Injection into Helical Device; Aug. 1999

NIFS-608 R. Tanaka, T. Nakamura and T. Yabe,
Constructing Exactly Conservative Scheme in Non-conservative Form; Aug. 1999

NIFS-609 H. Sugama,
Gyrokinetic Field Theory; Aug. 1999

NIFS-610 M. Takechi, G. Matsunaga, S. Takagi, K.Ohkuni, K. Toi, M. Osakabe, M. Isobe, S. Okamura, K. Matsuoka, A. Fujisawa, H. Iguchi, S. Lee, T. Minami, K. Tanaka, Y. Yoshimura and CHS Group,
Core Localized Toroidal Alfven Eigenmodes Destabilized By Energetic Ions in the CHS Heliotron/Torsatron; Sep. 1999

NIFS-611 K. Ichiguchi,
MHD Equilibrium and Stability in Heliotron Plasmas; Sep. 1999

NIFS-612 Y. Sato, M. Yokoyama, M. Wakatani and V. D. Pusovitov,
Complete Suppression of Pfirsch-Schluter Current in a Toroidal l=3 Stellarator; Oct. 1999

NIFS-613 S. Wang, H. Sanuki and H. Sugama,
Reduced Drift Kinetic Equation for Neoclassical Transport of Helical Plasmas in Ultra-low Collisionality Regime; Oct. 1999

NIFS-614 J. Miyazawa, H. Yamada, K. Yasui, S. Kato, N., Fukumoto, M. Nagata and T. Uyama,
Design of Spheromak Injector Using Conical Accelerator for Large Helical Device; Nov. 1999

NIFS-615 M. Uchida, A. Fukuyama, K. Itoh, S.-I. Itoh and M. Yagi,
Analysis of Current Diffusive Ballooning Mode in Tokamaks; Dec. 1999

NIFS-616 M. Tanaka, A.Yu Grosberg and T. Tanaka,
Condensation and Swelling Behavior of Randomly Charged Multichain Polymers by Molecular Dynamics Simulations; Dec. 1999